# **GEOSPHERE**

GEOSPHERE; v. 14, no. 6

https://doi.org/10.1130/GES01676.1

13 figures; 1 plate; 2 tables; 1 set of supplemental files

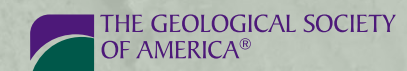
CORRESPONDENCE: tswaldien@ucdavis.edu

CITATION: Waldien, T.S., Roeske, S.M., Benowitz, J.A., Allen, W.K., Ridgway, K.D., and O'Sullivan, P.B., 2018, Late Miocene to Quaternary evolution of the McCallum Creek thrust system, Alaska: Insights for ange-boundary thrusts in transpressional orogens: Geosphere, v. 14, no. 6, p. 2379–2406, https://doi.org/10.1130/GES01676.1.

Science Editor: Raymond M. Russo Guest Associate Editor: James V. Jones III

Received 6 February 2018
Revision received 5 June 2018
Accepted 30 August 2018
Published online 19 October 2018





This paper is published under the terms of the CC-BY-NC license.

© 2018 The Authors

# Late Miocene to Quaternary evolution of the McCallum Creek thrust system, Alaska: Insights for range-boundary thrusts in transpressional orogens

Trevor S. Waldien<sup>1</sup>, Sarah M. Roeske<sup>1</sup>, Jeffrey A. Benowitz<sup>2</sup>, Wai K. Allen<sup>3</sup>, Kenneth D. Ridgway<sup>3</sup>, and Paul B. O'Sullivan<sup>4</sup>

Department of Earth and Planetary Sciences, University of California, Davis, 1 Shields Avenue, Davis, California 95616, USA

<sup>2</sup>Geophysical Institute, University of Alaska, Fairbanks, 900 Yukon Drive, Fairbanks, Alaska 99775, USA

<sup>3</sup>Earth, Atmospheric, and Planetary Sciences, Purdue University, 550 Stadium Mall Drive, West Lafayette, Indiana 47907, USA

<sup>4</sup>GeoSep Services, 1521 Pine Cone Road, Moscow, Idaho 83843, USA

#### **ABSTRACT**

Thrust systems are a primary mechanism for accommodating the convergent component of oblique plate motion and are therefore key players in the structural development of transpressional orogens. In southern Alaska, the Denali fault system is a highly partitioned dextral-convergent fault system spatially coincident with Alaska Range topography and thus offers an opportunity to evaluate the evolution of range-bounding thrust systems in orogens resulting from oblique plate motion. Our analysis is focused on the late Miocene-Present McCallum Creek thrust system, which consists of the McCallum Creek reverse fault and a kinematically linked foreland thrust system south of the Denali fault in the eastern Alaska Range. Apatite fission-track cooling ages, tephrachronology, and balanced cross sections indicate that convergence partitioned to the McCallum Creek thrust system has accommodated ~4 km of rock exhumation and ~5.5 km of south-vergent shortening since hanging wall rocks passed through the apatite fission-track partial annealing zone at ca. 6 Ma. A blind foreland thrust system developed after ca. 3.8 Ma and was subsequently overtaken by out-of-sequence slip on the main McCallum Creek fault. Incised segments of modern streams, perched terraces, and tilted Quaternary deposits suggest that foreland structures are active in the Quaternary. Shortening on the McCallum Creek thrust system is oriented at a high angle to the Denali fault, making the McCallum Creek thrust system one of the only known structures south of the Denali fault in the Alaska Range to accommodate the collisional mode of active deformation in southern Alaska. The late Miocene reactivation of faults in the McCallum Creek area likely records evolution of the Denali fault system in response to modification of the southern Alaska convergent plate boundary.

#### INTRODUCTION

Thrust faults have been identified as key structures contributing to topographic development and basin evolution in long-lived strike-slip fault systems (Meisling and Weldon, 1989; Erdman and Kelsey, 1992; Yin et al., 2002). Often,

regions experiencing oblique convergence give rise to an active transpressional orogen wherein the components of overall plate motion are partitioned into a central strike-slip fault with thrust faults at the topographic margins of the range (e.g., the California Coast Ranges; Unruh and Moores, 1992). In theoretical and analog models of oblique convergence, shortening structures are observed to develop both parallel and oblique to the master strike-slip fault, which has been interpreted to reflect the convergence angle of relative plate motion (Sanderson and Marchini, 1984; Tikoff and Peterson, 1998). Natural orogens accommodating oblique convergence contain active shortening structures at variable orientation with respect to the master strike-slip fault (e.g., Stein and Ekström, 1992), which may reflect a more complicated relationship between convergence angle and the orientation of contractional structures. Furthermore, the magnitude of fault-normal plate motion may change along strike of the strike-slip fault system (e.g., Little et al., 2005; Spotila et al., 2007), which predicts that thrusts may form continually during evolution of the fault system and that the relative importance of existing thrusts may change as they are translated along strike. Thus, a time-integrated model of thrust system development in the context of strike-slip translation and fault system evolution is necessary to better understand the spatial and temporal changes in strain accumulation, seismicity patterns, topographic growth, and basin development in obliquely convergent tectonic settings.

Transecting southern Alaska, the Alaska Range is the topographic expression of the Denali fault system, a Cenozoic dextral-convergent fault system (e.g., Richter and Matson, 1971). Approximately 20% of the modern Pacific–North America (PAC-NAM) relative plate motion is transferred from the southern Alaska convergent plate margin inboard to the Denali fault system (cf. Matmon et al., 2006; Elliott et al., 2013) (Fig. 1). Oblique convergence across the Denali fault system is accommodated by dextral slip on the master Denali fault and thrusting on faults at the northern (Bemis and Wallace, 2007; Burkett et al., 2016) and southern (Haeussler, 2008; Riccio et al., 2014) margins of the Alaska Range. Thrusts in the Northern Foothills fold and thrust belt strike subparallel to the curved Denali fault and record 1–4 mm/yr of Denali fault-normal convergence north of the Denali fault (Bemis et al., 2015). At the southern margin

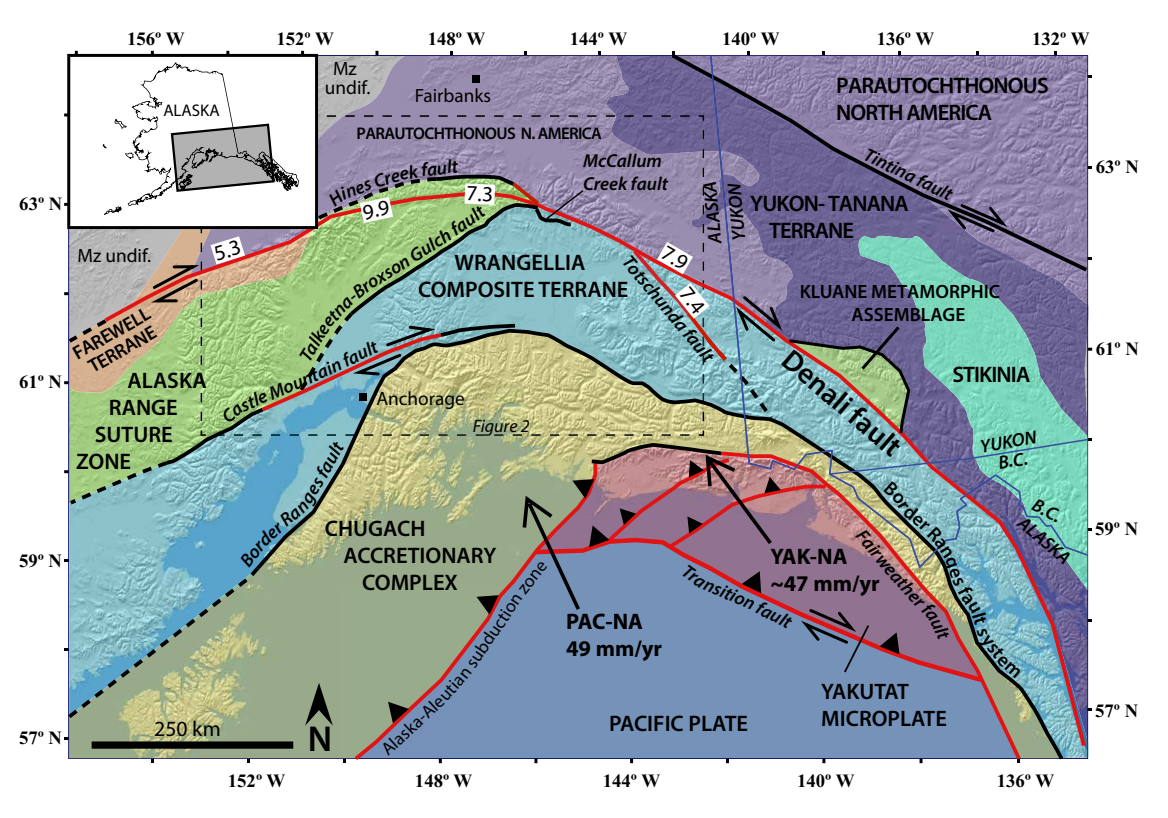


Figure 1. Hillshade map showing the McCallum Creek fault relative to terrane geology and the key tectonic boundaries in southern Alaska and adjacent Canada. Terrane geology is simplified from Colpron and Nelson (2011). Red fault sections have known Quaternary slip (Koehler, 2013). Sections of the Denali and Totschunda faults are annotated with the average geologic slip rates (in mm/vr) from Haeussler et al. (2017b). The Yakutat (YAK)-North America (NA) relative plate motion vector is from Fletcher and Freymueller (2003). and the Pacific (PAC)-North America vector is from Eberhart-Phillips et al. (2006). The area of Figure 2 is outlined. B.C.-British Columbia; MZ undif.-Mesozoic undifferentiated

of the Alaska Range, thrust faults west of 145.7°W (the Delta River) generally strike oblique to the Denali fault and are interpreted to accommodate counterclockwise rotation of the crust south of the fault (Stout and Chase, 1980; Haeussler, 2008) (Fig. 2). To the east of 145.7°W, one range boundary thrust south of the Denali fault, the McCallum Creek fault, strikes parallel to the Denali fault and accommodates late Cenozoic Denali fault-normal shortening (Ridgway et al., 2002). The variable orientation of thrust faults south of the Denali fault implies that they generally accommodate contrasting modes of regional block motion: Denali fault-normal contraction east of 145.7°W and rotation-related convergence to the west. Understanding the activity of these variably oriented thrust faults through time and how they interact to accommodate relative plate motion requires knowledge of fault kinematics, geometry, and timing of slip.

Here, we present new geologic mapping, structural data, and six new apatite fission-track (AFT) cooling ages from plutonic and low-grade metavolcanic rocks to reveal the late Miocene–Quaternary shortening history for the Mc-Callum Creek fault and a kinematically linked system of blind thrust faults deforming the foreland basin. Acknowledging that the McCallum Creek fault has experienced earlier phases of slip (e.g., Terhune et al., 2015; Benowitz et al.,

2015), our description of the McCallum Creek thrust system herein refers only to convergent deformation that occurred from the late Miocene to Quaternary. We deduce a sequence of events describing the evolution of the thrust system, integrate our findings with other geologic data to estimate the rate of Denali fault-normal convergence east of 145.7°W, and propose features of the thrust system that may inform analyses of thrust systems in other orogens responding to obliquely convergent plate motion.

#### ■ REGIONAL GEOLOGIC CONTEXT

#### **Architecture of the Denali Fault System**

The Denali fault system is an active dextral-convergent fault system, which primarily occupies the suture between pericratonic metamorphic terranes in the north and allochthonous oceanic terranes in the south (Fitzgerald et al., 2014) (Fig. 1). East of 145.7°W, the Denali fault system predominately juxtaposes 35–40 km thick mafic crust of the Wrangellia island arc terrane against

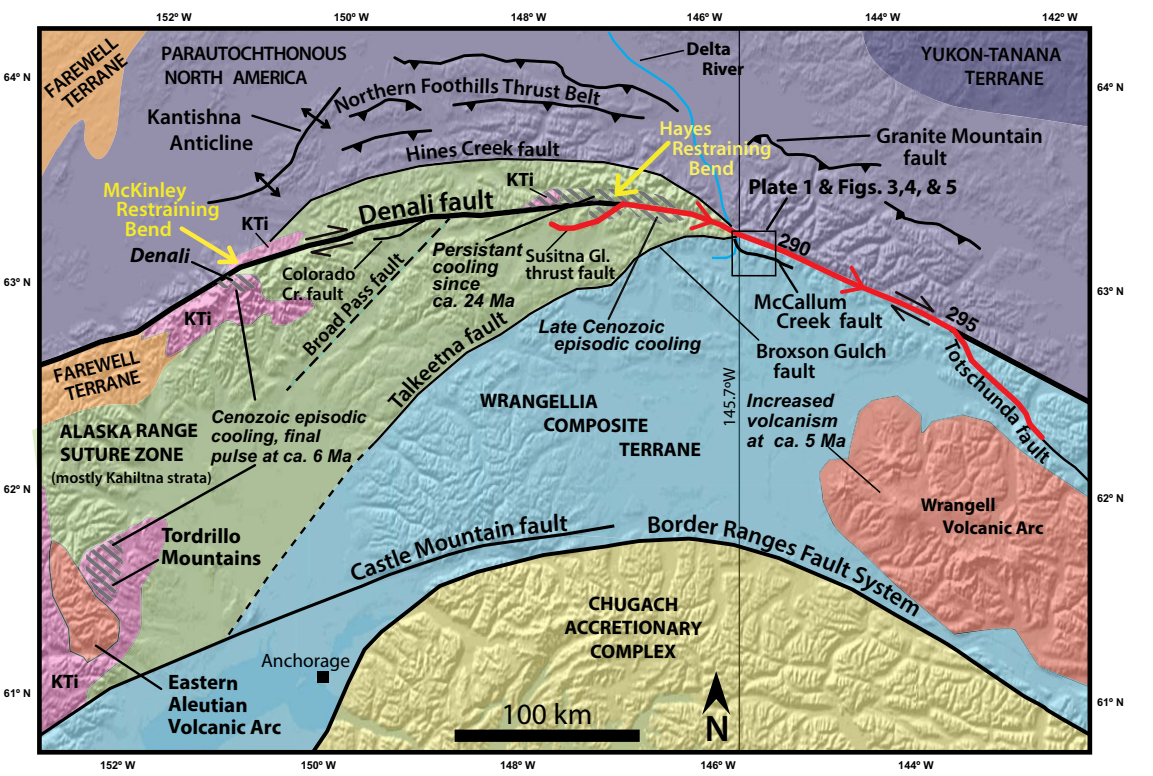


Figure 2. Hillshade map of the Alaska Range and the surrounding region overlain by terrane geology and major tectonic boundaries generalized from Wilson et al. (2015) and Colpron and Nelson (2011). Locations where low-temperature thermochronometry has been applied to the Alaska Range are annotated with diagonal stripes. The cooling trend for the Tordrillo Mountains is from Benowitz et al. (2012) (apatite fission-track [AFT] and 40Ar/39Ar K-feldspar) and Haeussler et al. (2008) (AFT and apatite (U-Th)/He [AHe]). The cooling trend in the Denali area is from Fitzgerald et al. (1993: 1995) (AFT) and Perry (2014) (AFT and AHe). Cooling trends north and south of the Hayes restraining bend are from Benowitz et al. (2011, 2014) (40Ar/39Ar muscovite, biotite, and K-feldspar, AFT, and AHe), Perry (2014) (AFT and AHe), and Riccio et al. (2014) (AFT and AHe). Volcanic productivity in the Wrangell arc is from Preece and Hart (2004). Red line is the trace of the surface rupture from the 2002 M., 7.9 Denali earthquake with arrows indicating rupture propagation direction (Eberhart-Phillips et al., 2003). The strike of the Denali fault at locations north of the McCallum Creek area and at the Denali-Totschunda intersection are given on the northern side of the fault. KTi - Cretaceous-Cenozoic plutons emplaced along the Denali fault, which are generally targeted for low-temperature thermochronology. The Kahiltna basin mentioned in the text occupies much of the Alaska Range suture zone crust. The study area is the area of Figures 3, 4, 5, and Plate 1.

~30 km thick felsic crust of the parautochthonous North American continental margin (Nokleberg et al., 1982; Dusel-Bacon et al., 2017; Miller et al., 2018) (Fig. 2). Localized fault-bounded packages of Late Jurassic-Cretaceous marginal marine strata (Kahiltna basin) also crop out along this section of the fault (Wilson et al., 2015). West of 145.7°W, the Denali fault intersects a large region of tectonically thickened (~45 km) crust composed of Kahiltna strata, plutons, and miscellaneous crustal fragments within the Alaska Range suture zone (Ridgway et al., 2002; Brennan et al., 2011; Nokleberg et al., 2013) (Fig. 2). Our study area is at the transition between these two regions of contrasting geology and crustal structure.

Thrust systems north and south of the Denali fault are responsible for outward expansion of Alaska Range topography (Bemis and Wallace, 2007; Riccio et al., 2014; Bemis et al., 2015; Terhune et al., 2015). The Northern Foothills fold and thrust belt comprises a series of north-vergent thrusts and backthrusts, which accommodate Pliocene-Present convergence at the northern margin of the Alaska Range (Bemis and Wallace, 2007) (Fig. 2). South of the Denali fault, the Cenozoic history of convergence is poorly understood. From west to east, potentially significant Cenozoic shortening structures south of the Denali fault include the Colorado Creek, Broad Pass, Susitna Glacier, Broxson Gulch, and McCallum Creek faults (Haeussler, 2008; Haeussler, et al., 2017a, 2017b) (Fig. 2). Oligocene slip on the Colorado Creek thrust fault (Trop et al., 2004, 2014), Neogene-Quaternary slip on the Broad Pass fault (Haeussler et al., 2017a), Neogene and historic activity on the Susitna Glacier thrust fault (Crone et al., 2004; Riccio et al., 2014), Cenozoic and historic(?) activity on the Broxson Gulch fault (Stout and Chase, 1980; Doser, 2004; Waldien et al., 2016), and late Miocene-Present activity on the McCallum Creek fault (Weber and Turner, 1977; Ridgway et al., 2002; Benowitz et al., 2007; this study) show that splay faults on the south side of the Denali fault also accommodate significant Cenozoic shortening across the Alaska Range orogen.

# Late Cenozoic Exhumation and Shortening in the Alaska Range

Low-temperature thermochronometry, often applied to Cretaceous and Cenozoic plutonic rocks in the Alaska Range, has helped elucidate the spatial and temporal distribution of strain accommodation within the Denali fault SUPPLEMENT SI: FAULTKIN METHODOLOGY

Slickenlines and slickenfibers record one phase of slip on an individual fault plane 4 the Mohr-Coulomb criterion), the statistical analysis of populations of slickenlines with minor 5 displacements on a large number of differently oriented brittle faults can be averaged to infer the 6 orientation of the principal incremental strain axes describing the deformation and thereby give 7 insight into the recorded kinematic history of brittle faulting (Gapais et al., 2000; Twiss and

10 plane solution) of the principal extension (T) and shortening (P) axes for a given population of 11 faults. Input parameters include the orientation, slip direction (rake), and sense of slip for each 12 fault plane, which are measured from the outcrop. We ranked the kinematic measurements based 13 on our confidence in the accuracy of each interpretation: 'A' (sure of the interpretation), 'B' (reasonably sure of the interpretation), or 'C' (not sure of the interpretation). These data are input raction (P) for each fault plane are determined by assuming they are oriented at 45 degrees to 17 the slip vector and contained within a plane perpendicular to the fault plane (Marrett and 18 Allmendinger, 1990). Faultkin contours the T and P axes of the population of faults using the 19 Kamb (1959) method and divides the contoured T and P axes using the Angelier (1979) method 20 for calculating T and P dihedra (Marrett and Allmendinger, 1990). The result of these 21 calculations is a graphical representation of the deformation recorded by all input fault planes 22 (fault plane solution). We interpret these fault plane solutions to represent the kinematics of the 23 fault zone at the location of field measurements. In our analyses, including 'C' and 'B' 24 confidence level measurements did not significantly change the output fault plane solution, so we

<sup>1</sup>Supplemental Files. Geochronology methods, structural analysis methods, and detailed map. Please visit https://doi.org/10.1130/GES01676.S1 or access the full-text article on www.gsapubs.org to view the Supplemental Files.

25 include the low-confidence measurements in our analysis. We use our geologic mapping to

26 identify the appropriate nodal plane of the resulting fault plane solution as the fault plane.

system (Fig. 2). K-feldspar (closure temperature [T<sub>c</sub>] ~350-150 °C; Lovera et al., 2002) and muscovite (T<sub>c</sub> ~400 °C; Harrison et al., 2009) <sup>40</sup>Ar/<sup>39</sup>Ar thermochronometry shows the onset of rapid (~20-25 °C/m.y.) cooling of rocks north of the Denali fault near the Hayes restraining bend starting at ca. 24 Ma and is attributed to flat-slab subduction of the Yakutat (YAK) microplate at the southern Alaska plate margin (Benowitz et al., 2011; 2014) (Fig. 2). Apatite fission-track (T<sub>c</sub> ~120-100 °C; Gallagher et al., 1998) and apatite (U-Th)/He (AHe) (T<sub>c</sub> ~75-70 °C; Wolf et al., 1996) ages on rocks north of the Hayes restraining bend show that this long-term cooling trend is also documented in lower-temperature thermochronometers (Benowitz et al., 2011; Perry, 2014).

Low-temperature cooling ages from previous studies show localized episodic Neogene exhumation in regions of the Alaska Range south of the Denali fault. Apatite fission-track and AHe cooling ages near Denali in the central Alaska Range show slower (~15 °C/m.y.) cooling starting in the late Oligocene transitioning to rapid (~30 °C/m.y.) cooling at ca. 6 Ma (Fitzgerald et al., 1993, 1995; Benowitz et al., 2012; Perry, 2014; Burkett et al., 2016) (Fig. 2). K-feldspar <sup>40</sup>Ar/<sup>39</sup>Ar, AFT, and AHe cooling ages from the Tordrillo Mountains in the western Alaska Range show a complicated cooling path starting in the Eocene and switching to rapid (~20 °C/m.y.) cooling at ca. 6 Ma (Haeussler et al., 2008; Benowitz et al., 2012). The location of these young cooling ages in areas of high topographic relief and near mapped faults suggests that slip on structures in the Denali fault system near the margin of high topography facilitates rock uplift, rapid erosion, and resulting exhumation. As a result, locations with rapid Cenozoic bedrock cooling in the Alaska Range likely record slip on structures that accommodate far-field deformation from the southern Alaska convergent margin.

Thrust faults south of the Denali fault in the eastern Alaska Range have been suspected to be important Neogene convergent structures (Stout and Chase, 1980; Plafker et al., 1994; Ridgway et al., 2002). Initiation of the 2002 M<sub>w</sub> 7.9 Denali earthquake on the Susitna Glacier thrust fault (Eberhart-Phillips et al., 2003; Crone et al., 2004; Haeussler et al., 2004) prompted examination of the Neogene exhumation history for this structure (Riccio et al., 2014). Apatite fission-track and AHe cooling ages from across the Susitna Glacier thrust indicate that it has not facilitated significant exhumation since the mid-Miocene (Riccio et al., 2014), and low-temperature cooling ages from the south side of the Hayes restraining bend show only minor regional exhumation since ca. 15-20 Ma (Benowitz et al., 2011, 2014; Perry, 2014; Waldien et al., 2017). Conversely, the steep topographic gradient across the McCallum Creek fault trace (>1000 m of relief in less than ~2 km distance) and deformed, and locally overturned, Pliocene strata (Ridgway et al., 2002; Allen, 2016) in the footwall of the fault illuminate this structure as a potentially significant Pliocene-Quaternary shortening structure at the southern margin of the Alaska Range.

#### The McCallum Creek Fault

The McCallum Creek fault coincides with a steep topographic gradient at the southern margin of Alaska Range east of the Delta River (Figs. 2 and 3) and, largely based on the lack of detailed studies, is listed as a "pre-Quaternary"

fault in the Alaska Division of Geological and Geophysical Surveys (DGGS) active fault database (Koehler, 2013). However, the steep topographic gradient across the fault trace and the abundance of aftershocks near the fault immediately following the 2002 M<sub>w</sub> 7.9 Denali earthquake suggest that the McCallum Creek fault is an active component of the Denali fault system, despite the lack of evidence for a surface rupture on the fault during the 2002 event (Ratchkovski et al., 2003, 2004; Haeussler et al., 2004). Alignment of aftershock hypocenters corroborates seismic reflection (Brocher et al., 2004), gravity, and magnetic (Fisher et al., 2004) data locating the McCallum Creek fault as a moderately N-dipping structure in the subsurface (Fig. 4). Apatite fission-track and AHe ages from crystalline bedrock in the hanging wall of the McCallum Creek fault show rapid cooling through the Pliocene (Perry, 2014; this study), coeval with foreland basin development in the footwall (Weber and Turner, 1977; Kunk, 1995; Allen, 2016). The folded late Miocene-Pliocene foreland strata contain material partially derived from the hanging wall of the fault (Allen, 2016). This sum of evidence suggests the McCallum Creek fault has been active as a thrust splaying from the Denali fault since at least the late Miocene. The Eocene to late Miocene history of this deformation zone is not a focus of this study but is currently being investigated (Terhune et al., 2015; Fitzgerald et al., 2017).

A reconstruction of the late Miocene-Quaternary evolution of the McCallum Creek thrust system is needed to: (1) better quantify the magnitude of active Denali fault-normal shortening across the Alaska Range east of 145.7°W; (2) provide additional boundary conditions to reconstruct upper-plate deformation in the southern Alaska convergent margin; and (3) better characterize the potential seismic hazard to citizens and infrastructure (Trans-Alaska pipeline, Richardson highway, etc.) in the region of the fault.

#### METHODS

#### Fault Kinematics

We used criteria outlined by Petit (1987) and Doblas (1998) to record and interpret brittle kinematic indicators at four locations in the damage zone of the McCallum Creek fault (locales 17ATW-16, 14ATW-42, 14ATW-23, and 14ATW-02 in Fig. 3). At each locale, we measured the shear plane surface orientation, brittle lineation rake within the shear plane, and slip sense on at least 20 surfaces within an ~10 m radius on the outcrop. We used FaultKin software (Marrett and Allmendinger, 1990; Allmendinger et al., 2012) to plot these fault-slip data and produce a fault-plane solution describing the fault kinematics for each locale (FaultKin methods in Supplemental File S11). Fault-plane solutions produced from fault zone slickenline measurements are referred to in the text as the "measured fault-plane solutions."

Because inversions of seismicity may reliably approximate the orientations of the strain rate axes for an associated deformation (Unruh et al., 1996), we compare our measured fault-plane solutions to inversions of his-

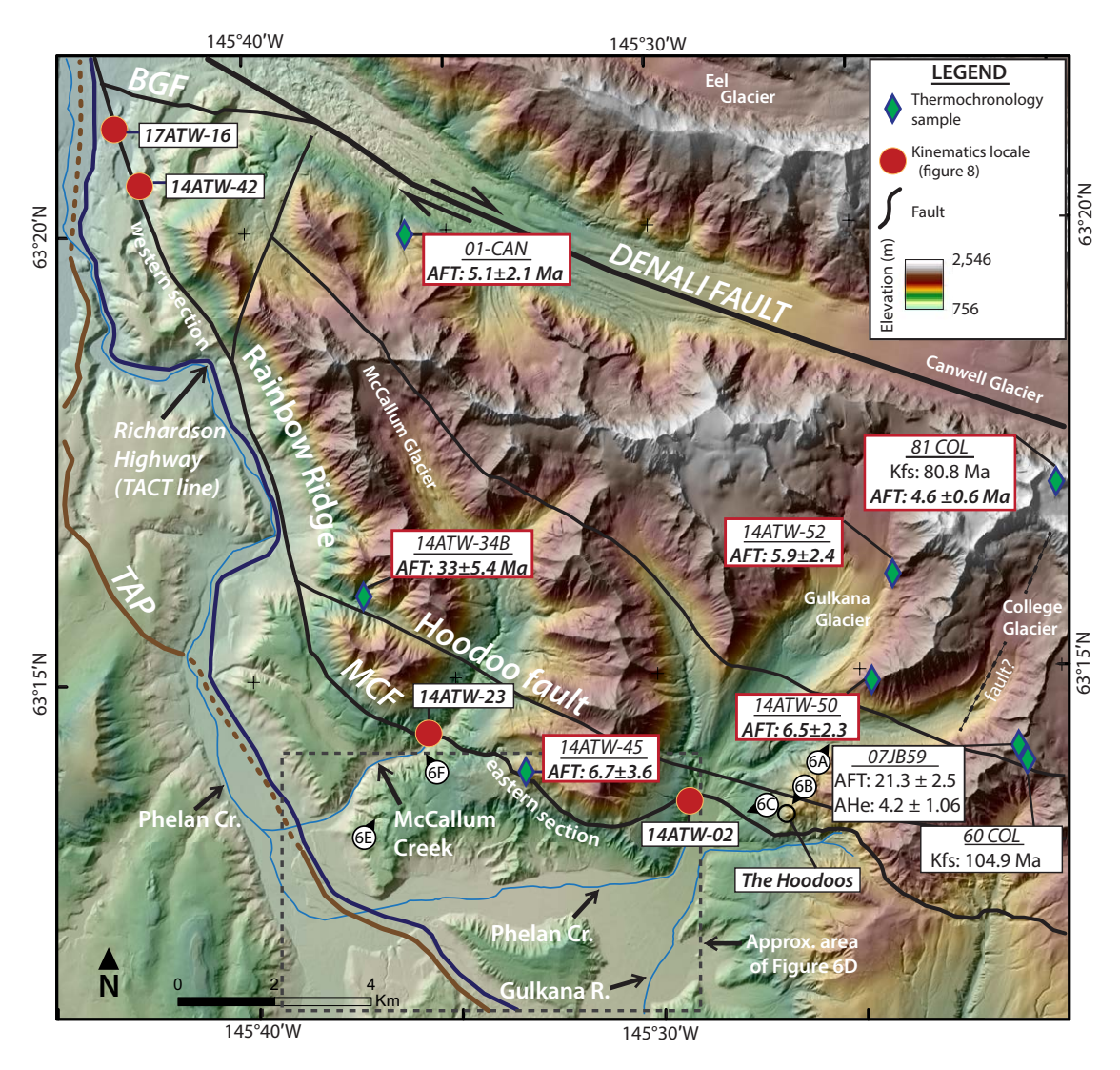


Figure 3. Shaded relief locale map with the same spatial extent as Plate 1 showing sample locations, ages, field photo locations, and geographic features relative to the McCallum Creek fault (MCF). Ages shown in bold font are not previously published, and those within a red box are used for thermal models (Fig. 10). K-feldspar ages at 81COL and 60COL are 40Ar/39Ar minimum ages published in Benowitz et al. (2014). Apatite-fission track (AFT; pooled age with 1σ uncertainty) and apatite (U-Th)/He (AHe; apatite (U-Th)/He ages averaged from multiple-grain aliquots with 2σ uncertainty) ages for sample 07JB59 are presented in Perry (2014). TAP-Trans-Alaska Pipeline (brown line), dashed where buried. TACT-Trans-Alaska Crustal Transect (dark blue line); BGF-Broxson Gulch fault.

toric seismicity in the region of the fault (Fig. 4). Ratchkovski et al. (2004) present a suite of stress-tensor inversions along strike of the Denali fault system for seismicity during two time periods: (1) leading up to the 2002 M<sub>w</sub> 7.9 Denali earthquake and (2) during and after the 2002 Denali earthquake. Ratchkovski et al. (2004) present these stress-tensor inversions as orientations of principal stress axes. Interpreting the inverted stress axes as strain rate axes (e.g., Twiss and Unruh, 1998), we construct a suite of fault-plane solutions using the trend of the principal shortening strain rate axis and the orientation of the McCallum Creek fault measured from the geologic map. In the following text, we refer to these fault-plane solutions as the "predicted fault-plane solutions." Comparing the measured and predicted fault-plane solutions allows us to test if the fault slip measured in the field is consistent with the current strain rate axis orientations on the McCallum Creek fault. Relating slickenline data to stress-tensor inversions from

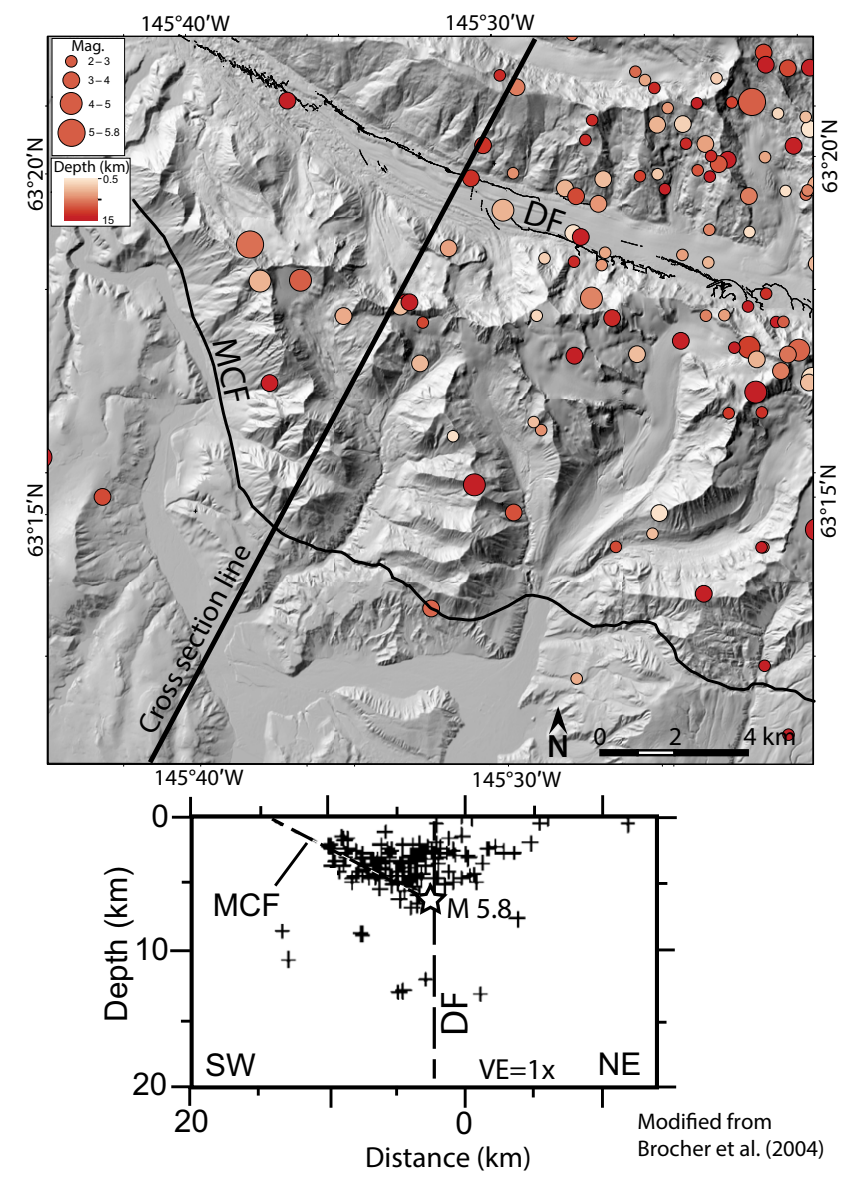


Figure 4. Hillshade map of the same aerial extent as Figure 3 showing all historic seismicity in the study area (2M 2.0 and 0.5–15 km depth) on record until 23 January 2018 (from U.S. Geological Survey Earthquake catalog: earthquake.usgs.gov/earthquakes/search). Cross section plot shows aftershocks from the 2002 Denali earthquake plotted as crosses (modified from Brocher et al., 2004; their cross section E). Earthquakes are projected to the cross section line from a 20 km wide area (Ratchkovski et al., 2003). DF—Denali fault (2002 rupture trace); MCF—McCallum Creek fault; VE—vertical exaggeration.

historic earthquakes assumes that the slickenlines exposed in the damage zone of the McCallum Creek fault formed during the most recent phase of slip for the fault and that the seismicity data used for stress-tensor inversions represent motion on the McCallum Creek fault through this phase of slip over geologic time. Acknowledging these assumptions, we compare measured fault-plane solutions to predicted fault-plane solutions in order to determine the convergence direction across the McCallum Creek fault since the late Miocene.

#### **Balanced Cross Sections**

Our new geologic mapping at 1:10,000 scale on base maps constructed from interferometric satellite aperture radar (IfSAR) Alaska digital terrain model data (~5 m raster resolution; ifsar.gina.alaska.edu) emphasizes the geometry of folds associated with the McCallum foreland thrust system and the relationship between these folds and the McCallum Creek fault. We used the trishear fault propagation fold function in the Move software package (www.mve.com) to iteratively produce forward kinematic models for cross sections A-G (Fig. 5; Plate 1). To quantify the amount of shortening absorbed by structures in the foreland thrust system, the cross sections are area balanced using the program AreaErrorProp (Judge and Allmendinger, 2011). Our area balancing approach incorporates adjustments to the taper and thickness of the initial stratigraphic wedge and décollement location to explore uncertainties within these parameters, resulting in a range of area-shortening values for each cross section. The suite of forward modeled cross sections bracket the minimum and maximum shortening magnitudes in the foreland thrust system. We selected a preferred model for each cross section, which adequately fits surface geologic data and has reasonable geometry in regions of no exposure. See Supplemental File S2 (footnote 1) for cross section model parameters and detailed methods.

# **Apatite Fission-Track Thermochronometry**

We use AFT thermochronometry to constrain the cooling history of six bedrock samples in the hanging wall of the McCallum Creek fault (samples 14ATW-34B, 14ATW-45, 14ATW-50, 14ATW-52, 81COL, and 01CAN; Fig. 3). The AFT system records cooling below temperatures of ~120–100 °C (Gallagher et al., 1998). All AFT analyses were performed using the laser ablation–inductively coupled plasma–mass spectrometry (LA-ICP-MS) method (Hasebe et al., 2004; Donelick et al., 2005) at GeoSep Services. Semiquantitative information regarding cooling rate and reheating conditions may be gleaned from tracklength distributions and fission-track orientation with respect to the crystallographic c-axis (e.g., Green et al., 1986; Donelick et al., 2005). See Supplemental File S3 (footnote 1) for standard sample preparation and LA-ICP-MS AFT methodology for GeoSeps Services.

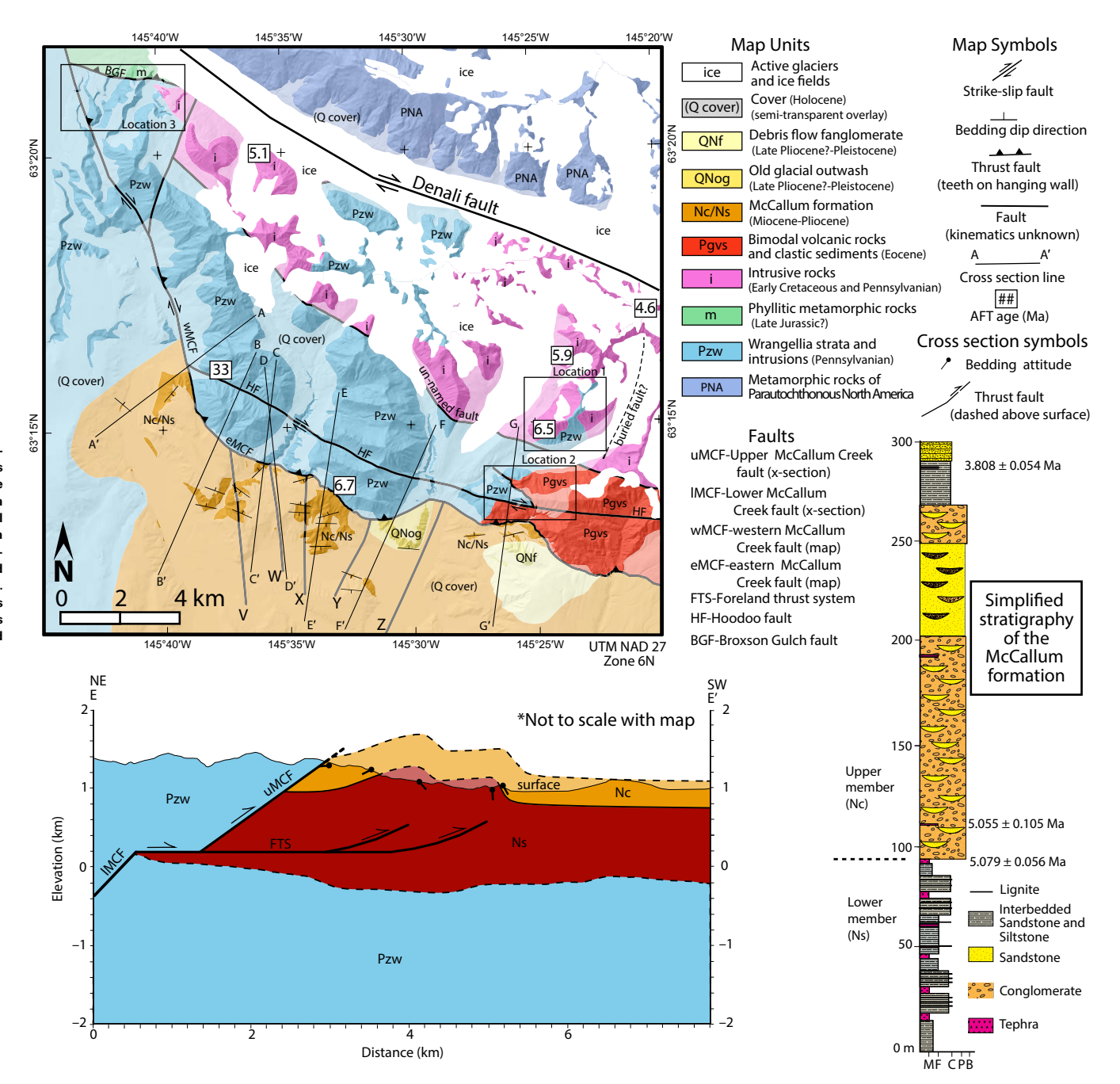
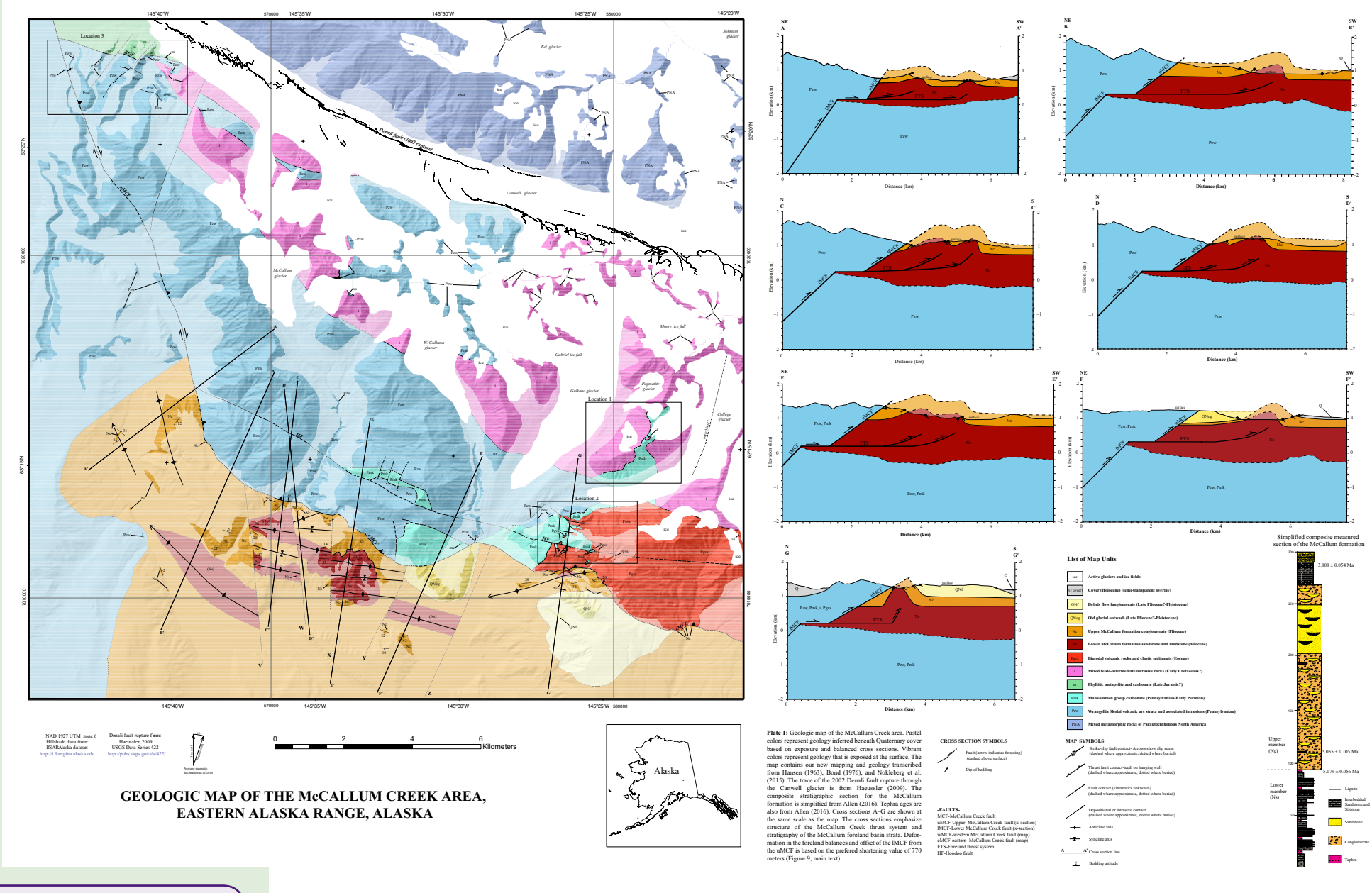


Figure 5. Simplified geologic map showing general map relationships, the areas of our focused mapping, average apatite fission-track (AFT) ages, and cross section lines. Cross section E shows the general structural style exhibited by the McCallum Creek thrust system. The simplified stratigraphy of the McCallum Formation and <sup>49</sup>Ar/<sup>39</sup>Ar tephra ages are from Allen et al. (2014) and Allen (2016). Plate 1 contains more detailed mapping and all of the cross sections (A–G). Tear faults in the foreland thrust system are labeled V–Z.

e/article-pdf/14/6/2379/4578814/2379.pdf



For the full-sized PDF file of Plate 1, please visit <a href="http://doi.org/10.1130/GES01676.p1">http://doi.org/10.1130/GES01676.p1</a> or the full text article on www.gsapubs.org.

Plate 1. Geologic map of the McCallum Creek Area, eastern Alaska Range, Alaska. For the full-sized PDF file of Plate 1, please visit http://doi.org/10.1130/GES01676.p1 or the full text article on www.gsapubs.org.

re/article-pdf/14/6/2379/4578814/2379.pdf

The AFT cooling age gives only the minimum time that a sample cooled below ~120–100 °C and therefore does not capture the complete thermal history. To produce a more complete thermal history of rocks in the hanging wall of the McCallum Creek fault, we performed thermal modeling using the HeFTy soft-ware (Ketcham, 2005), which incorporates single-grain AFT ages, measured confined track lengths, the kinetic parameter Dpar, thermal conditions from the existing geochronology, and the mean annual surface temperature. HeFTy, which fits cooling curves to the input criteria using a Monte Carlo randomization, ran for 20,000 model iterations for each sample. The cooling curves generated by HeFTy are compared to the input data and assigned a goodness of fit value of either "good" (GOF >0.5) or "acceptable" (GOF >0.05). HeFTy calculates a weighted mean cooling path from all model iterations with a GOF >0.05.

#### RESULTS

# Geology of the McCallum Creek Area— Review and New Field Observations

## Pennsylvanian-Eocene Bedrock Geology

Previously published geologic maps of the McCallum Creek area by Hanson (1963), Bond (1976), Nokleberg et al. (1982), and Nokleberg et al. (1992a) range in scale from ~1:40,000-1:250,000 and primarily emphasize pre-Oligocene Wrangellia bedrock exposed in both the hanging wall and footwall of the McCallum Creek fault. Wrangellia strata in the McCallum Creek area consist of the Pennsylvanian-Permian volcanic and clastic strata related to the Skolai arc, Permian Mankommen Group carbonate and clastic strata, and Triassic Nikolai flood basalt (Bond, 1973, 1976; Nokleberg et al., 1992a). Because Mankommen Group strata are volumetrically significant in the field area and Nikolai strata are not, we distinguish only the Mankommen Group from other Wrangellia strata in the map area (Plate 1). Small volume igneous bodies ranging from ultramafic to intermediate in composition intrude Skolai arc strata but are absent from Mankommen group strata (Bond, 1976). Granitoid plutons intrude and are faulted against the Pennsylvanian-Permian Wrangellia strata (Bond, 1976). The granitoid suite is not well dated; however, K/Ar hornblende ages of ca. 325 Ma and 110 Ma (Nokleberg et al., 1992b) suggest that the plutonic complex has both a Pennsylvanian component related to the Skolai arc and an Early Cretaceous component related to the Chisana arc, which is described farther to the east within Wrangellia (Richter, 1976; Trop et al., 2002). All Paleozoic-Triassic strata in the map area are unconformably overlain by and faulted against a suite of Eocene volcanic strata (Bond, 1976) (Fig. 5; Plate 1).

In our mapping (Plate 1), we fundamentally re-interpret the bedrock geology at three locations in the hanging wall of the McCallum Creek fault (Locations 1, 2, and 3 on Fig. 5 and Plate 1). At locations 1 and 2, we re-interpret relationships between map units. At location 3, we re-define metamorphic units to better define the location of the Broxson Gulch fault.

Location 1: Our mapping in the eastern portion of the field area shows that intermediate to felsic plutonic rocks intrude the Mankommen Group east of the Gulkana glacier (Fig. 6A). This contact was previously mapped as a fault (see Bond, 1976; Nokleberg et al., 2015); however, the non-planar nature of the contact, contact metamorphism of the Mankommen strata, and lack of continuous tectonized rock at the contact indicate this is an intrusive relationship. The contact between Wrangellia strata and the southern margin of the plutonic complex is a fault west of the Gulkana glacier. We interpret that this fault cuts the intrusive contact obliquely under Quaternary cover and continues to the southeast, juxtaposing the plutonic complex against Eocene volcanic rocks (Fig. 5; Plate 1).

Location 2: The eastern portion of the map area contains a bimodal volcanic and volcaniclastic unit in the hanging wall of the McCallum Creek fault. The volcanic rocks are dated at ca. 49 Ma (Bond, 1976; Nokleberg et al., 1992a). Bond (1976) mapped the Eocene volcanic unit as a number of fault-bounded blocks juxtaposed against the Mankommen Group and Nikolai greenstone. While these units are tectonically juxtaposed at some locales in the area, many of the contacts are non-planar surfaces where the poorly indurated Eocene volcanic unit surrounds a cliff of older Mankommen strata (Fig. 6B). Locally, the Eocene volcanic strata are topographically lower than and surrounded by outcrops of older strata on all sides. We interpret these map patterns to record deposition of the Eocene volcanic strata onto a landscape of incised valleys separated by ridges of Mankommen Group strata. The Eocene volcanic rocks are likely internally faulted and folded. However, the complex volcanic stratigraphy and poor induration make these structures cryptic. Resolving the volcanic stratigraphy to better understand the structure within the Eocene volcanic unit is not part of our analysis but is a focus of ongoing research (Fitzgerald et al., 2017). We acknowledge that the Cenozoic tectonic evolution of southern Alaska has resulted in long-lived deformation zones with polyphase slip histories (e.g., Betka et al., 2017; Rosenthal et al., 2017). The Eocene bimodal volcanic strata in the hanging wall of the McCallum Creek fault may record that extension was the dominant deformation style in the McCallum Creek area during the Eocene (e.g., Terhune et al., 2015).

Location 3: The northwestern corner of the map area contains metamorphic rocks with a variety of protolith compositions. These metamorphic rocks have been grouped into a single map unit on all previous maps. In our mapping, we observe that a ~30 m thick brittle shear zone intersects the metamorphic rocks and coincides with a major break in protolith composition. Rocks north of the brittle shear zone primarily have protolith compositions of graywacke and mudstone with subordinate carbonate. Rocks to the south are metamorphosed from mafic and ultramafic igneous rocks. Based on mapping, petrography, and geochronology from rocks west of the Delta River (Stout, 1965; Waldien et al., 2016), we interpret the brittle shear zone juxtaposing metamorphic rocks in the northwest corner of the map area as the Broxson Gulch fault. A set of NE-striking tear faults offsets the Broxson Gulch fault with apparent sinistral separation (Plate 1). The orientation and sense of separation on the tear faults are consistent with ~N-S convergence across the Broxson Gulch fault.

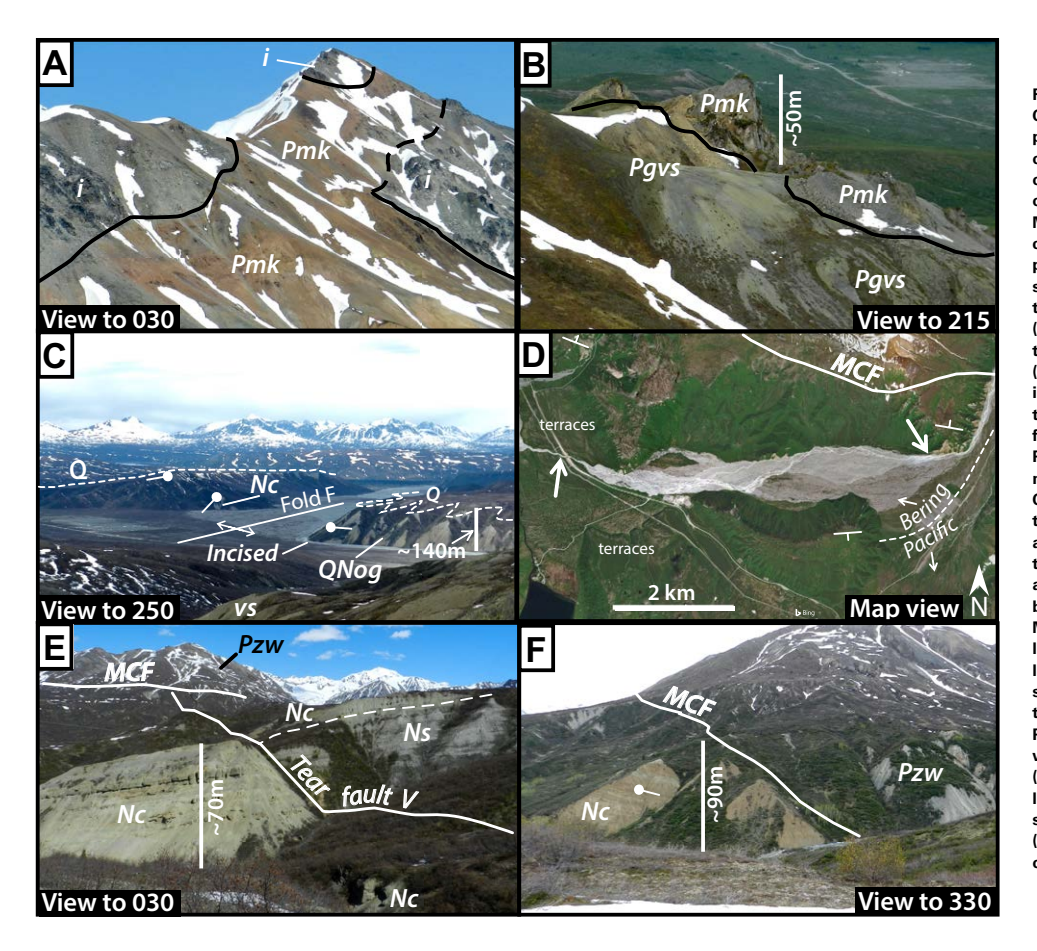


Figure 6. Field photos of geologic features in the McCallum Creek area. Azimuths of all photograph views are given, and photo locations are shown on Figure 3. (A) Granitoids (i-gray outcrops) intruding the Mankommen Group strata (Pmk-red outcrop) in the hanging wall of the McCallum Creek fault east of the Gulkana glacier. (B) Erosion-resistant carbonates of the Mankommen Group (Pmk) surrounded by poorly indurated Eocene volcanic rocks (Pgvs). The carbonate pillars shown in this photo are named "The Hoodoos." (C) Tilted glacial outwash strata (Q) unconformably overlaying upper McCallum Formation strata (Nc) in the forelimb of the fold in cross section F (left side of photo) and incised segment of Phelan Creek in the backlimb of the fold. The glacial outwash surficial deposit (Q) unconformably overlays an older glacial deposit (QNog) in the backlimb of the fold in cross section F. Glacial strata in the backlimb of the fold either dip modestly northward or are flat-lying. Bedding dip symbols are the same as Figure 5 and Plate 1. (D) Satellite image (from Bing) showing incised segments of Phelan Creek (large arrows) in the footwall of the Mc-Callum Creek fault. The eastern incised segment is deflected to the west creating the drainage divide between the Bering Sea and Pacific Ocean. The drainage divide may be structurally controlled by a tear fault between cross sections F and G (cf. Fig. 5 and Plate 1). Tilted glacial outwash strata are annotated with bedding attitude symbols. (E) A tear fault juxtaposes the upper McCallum Formation conglomerate (Nc) against lower McCallum Formation sandstone (Ns). Strata dipping ~20°N on the left side of the photo are in the backlimb of the fold in cross section B (Plate 1). Strata dipping ~17°N on the right are in the backlimb of the southern fold in cross section C (Plate 1). Paleozoic Wrangellia strata (Pzw) are exposed in the hanging wall of the McCallum Creek fault (MCF) in the background. (F) Paleozoic Wrangellia rocks (Pzw) thrust on top of McCallum Formation conglomerate (Nc). The dipping conglomerate strata are in the backlimb of the northern fold in cross section C (Plate 1). Geologic map unit labels are presented in the legend of Figure 5 and Plate 1.

#### Miocene-Pliocene Foreland Basin Strata

Mapping presented here (Fig. 5; Plate 1) focuses on the stratigraphy and structure of the McCallum foreland basin strata exposed in the footwall of the McCallum Creek fault. These Miocene-Pliocene strata consist of a lower mudstone-rich member and an upper gravel-rich member, collectively referred to herein as the McCallum Formation.

The lower member of the McCallum Formation consists of poorly indurated, well bedded lithic rich sands and muds with intercalated tephras and abundant lignite (Allen, 2016). Only ~100 m of the lower member are exposed in the map area, but the strata are more exposed along strike to the east (Allen, 2016), and the total thickness is likely ≥1000 m based on reflection seismology (Brocher et al., 2004) and gravity (Morin and Glen, 2003) observations from the Trans-Alaska Crustal Transect (TACT line shown in Fig. 3). Although the base of the lower member is not exposed, it likely unconformably overlays Paleozoic-Cenozoic strata equivalent to those exposed in the hanging wall of the McCallum Creek fault (Brocher et al., 2004). Because the base is not exposed, the timing of initial deposition of the McCallum Formation is unknown. However, volcanic ash beds in the lower member of the McCallum Formation indicate deposition into the basin was underway by ca. 6 Ma (Kunk, 1995; Benowitz et al., 2007; Allen, 2016).

The upper member of the McCallum Formation conformably overlies the lower member and consists of moderately well bedded coarse gravels with intercalated sand lenses, minor lignite, and tephra (Allen, 2016). A composite measured stratigraphic section suggests that ~215 m of the upper member are exposed in the footwall of the McCallum Creek fault in the map area (Allen et al.,

2014) (Fig. 5), but geologic mapping (Plate 1) suggests the preserved thickness may be as much as 400 m near the McCallum Creek fault and the unit thins toward the south. The lower ~215 m of the upper member is conformable with no evidence for growth strata (Allen, 2016).  $^{40}$ Ar/ $^{39}$ Ar tephrachronology brackets the onset of conglomerate deposition at ca. 5 Ma (Kunk, 1995; Benowitz et al., 2007; Allen, 2016). A 3.80 ± 0.05 Ma ( $^{40}$ Ar/ $^{39}$ Ar glass) tephra bed ~200 m above the base of the upper member indicates conformable deposition of the conglomerate lasted at least until this time (Allen, 2016) (Fig. 5; Plate 1).

Plio-Pleistocene(?) deposits overlie the upper member of the McCallum Formation. One Plio-Pleistocene deposit (map unit QNog, Fig. 5; Plate 1) is tilted ~6°N in the Gulkana glacier valley (cross section F). The contact between the upper McCallum Formation and this Plio-Pleistocene glacial unit is not exposed but is hypothesized to be an angular unconformity. A coarse, clast supported, poorly sorted, and poorly bedded unit interpreted to be a debris flow fanglomerate (map unit QNf) overlies the upper McCallum Formation in the eastern portion of the field area at cross section G (Fig. 5; Plate 1). Crude bedding in the fanglomerate dips up to 32°S, similar to the underlying upper McCallum Formation in this location. Because debris flow deposits may be emplaced with several degrees of dip (Hooke, 1968; Whipple and Dunne, 1992), it is possible that the fanglomerate was deposited with a significant initial dip. This would imply that the contact between the fanglomerate and upper Mc-Callum Formation is an angular unconformity and that the fanglomerate is sourced from the north. However, the contact between the fanglomerate and upper McCallum Formation is not well exposed, making this interpretation speculative.

# **Quaternary Geology**

Holocene(?) glacial and modern alluvial deposits unconformably overlie much of the bedrock geology in the McCallum Creek area. Because our analysis is primarily focused on the Neogene evolution of the McCallum Creek thrust system, we have lumped all surficial deposits on Figure 5 and Plate 1. A complete bedrock and surficial geologic map is forthcoming as another publication. We here describe only the aspects of the surficial geology in the field area that are pertinent to the development of the McCallum Creek thrust system.

Glacial moraines unmodified by fluvial processes are only found in the hanging wall of the McCallum Creek fault near the Gulkana and College glaciers (Fig. 3; Plate 1). Much of the geology in the footwall of the McCallum Creek fault is capped by a proglacial outwash deposit up to ~20 m thick. Crude stratigraphy in this outwash deposit is tilted ~5°N along cross section B and up to ~10°S along cross section F (Fig. 6C; Plate 1). It is beyond the scope of this paper to determine if this tilted bedding is coupled to a warped paleosurface. However, topographic analysis of the southern tip of cross section F using the IfSAR Alaska digital terrain model reveals that the modern surface is tilted ~8°–12°S, similar to the dip of crude bedding in the glacial outwash at this location (Waldien, 2015).

The modern drainage system, consisting of Phelan Creek, McCallum Creek, and the Gulkana River, dissects the folded McCallum Formation strata (Fig. 3; Plate 1). Phelan Creek flows south from the Gulkana and College glaciers and turns abruptly west, becoming an axial drainage system in the foreland of the McCallum Creek fault. Phelan Creek abruptly transitions from a braided stream system to a single incised channel where it is diverted to flow westward at the location of cross section F and again near its confluence with McCallum Creek in cross section C (Figs. 3, 5, 6C, and 6D; Plate 1). At least six generations of fluvial terraces are perched adjacent to the incised stream segment at the confluence between Phelan and McCallum Creeks (Waldien, 2015) (Fig. 6D). Phelan Creek continues to flow to the northwest before joining the Delta River, which flows north through the Alaska Range to the Tanana River, Yukon River, and ultimately to the Bering Sea. The headwater stream of the Gulkana River flows west out of a small catchment near the Hoodoos (Fig. 3) and abruptly turns south away from Phelan Creek, eventually joining the Copper River to the south, which flows to the Pacific Ocean. The drainage divide between these two watersheds is a subtle NE-trending topographic high within a broad, vegetated alluvial plain (Figs. 3 and 6D).

# Fault Geometry

Our geologic mapping (Fig. 5; Plate 1) along the trace of the McCallum Creek fault and in the foreland reveals the architecture of the McCallum Creek fault and a system of imbricated blind thrusts in the foreland. The mapping shows the McCallum Creek fault changes orientation near the intersection with the Hoodoo fault, northwest of McCallum Creek. The NE-dipping western section of the fault marks an ~1000 m high escarpment (Rainbow Ridge, Fig. 3) and cuts through Paleozoic volcanic and related intrusive rocks of the Wrangellia terrane. The N-dipping eastern section of the McCallum Creek fault places Wrangellia rocks and Eocene volcanic rocks over the late Miocene-Pliocene McCallum Formation (Figs. 6E and 6F). Exposures of the McCallum Creek fault generally consist of a zone of damaged rock up to ~50 m wide in the hanging wall Wrangellia rocks and ~10 m wide in the footwall McCallum Formation. Our mapping shows that the eastern section of the McCallum Creek fault is generally planar over lengths of ~200 m, but the dip changes along strike. At the map scale, the fault crosscuts fold axes related to the McCallum foreland thrust system and locally thins the upper McCallum Formation conglomerate (see cross section G, Plate 1).

The map also shows that the foreland thrust system is only present in the footwall of the eastern section of the McCallum Creek fault and that the cross-sectional geometry of folds in the foreland thrust system changes along strike. The map shows that two folds are exposed at the surface in cross sections A, C, D, and E, while only one fold is exposed in cross sections B, F, and G (Plate 1). These folds generally classify as open to tight (cf. Fleuty, 1964). The field data show that strata in the backlimb of the northern folds in cross sections A, E, and F transition from flat lying in the north to N-dipping on the backlimb

of the fold. All S-dipping forelimbs, except for the fold in cross section G, are steeper than the N-dipping backlimbs. These observations of fold geometry together suggest that folds in the McCallum Formation record slip on an imbricate set of N-dipping blind thrust faults that step up from a décollement at depth. Backlimb dip magnitudes on folds in all of the cross sections generally range from ~15°–25°N (Fig. 7). Exposed forelimb strata in cross sections D, E, F, and G generally dip ~35°S but may have locally overturned beds in the core of folds (Fig. 7; Plate 1). The southernmost fold limbs in cross sections A, B, and C are either buried beneath Quaternary deposits or have been eroded by Phelan Creek. Fold axes throughout the McCallum foreland strata generally trend subparallel to the trace of the McCallum Creek fault. Fold trains in the foreland are commonly separated from each other by ~N-striking tear faults that truncate fold axes (Plate 1). Tear faults V and X are exposed in the field (Figs. 5 and 6E; Plate 1). Tear faults W, Y, and Z are inferred under Quaternary deposits due to

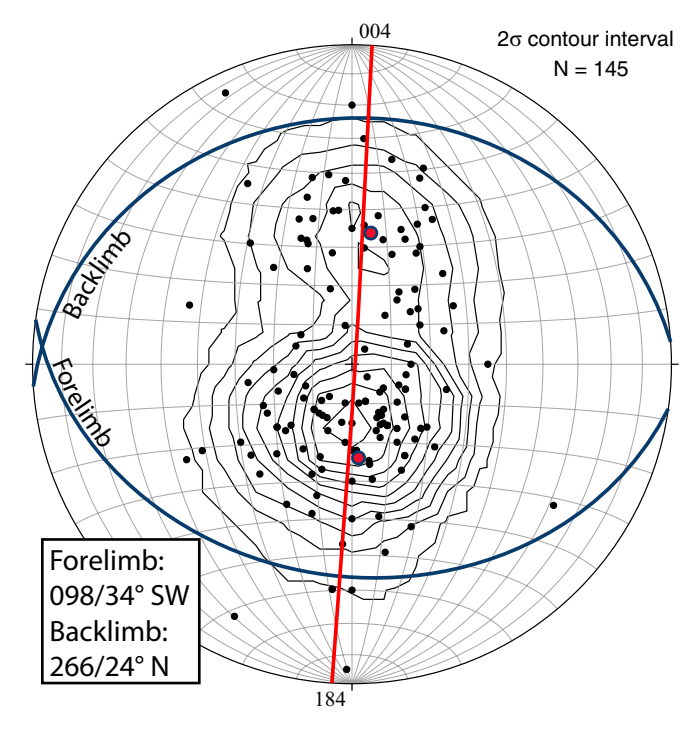


Figure 7. Lower hemisphere Schmidt projection of poles to bedding planes in the foreland basin strata (McCallum Formation) folded by the foreland thrust system contoured at 2¢ intervals using the method outlined in Kamb (1959). The red line is the cylindrical best fit to the data, which is subvertical and oriented along an azimuth of ~004–184, consistent with NNE-SSW shortening in the foreland thrust system. Blue great circles and corresponding poles represent averaged forelimb and backlimb orientations from the bedding attitude data, which are given in the lower left.

discontinuous fold axes along strike without a fold closure or reduction in the fold amplitude. Additionally, the location of tear fault Z is inferred due to the subtle NE-striking topographic barrier in the middle of the Gulkana glacier valley, which deflects the Gulkana River away from Phelan Creek (Fig. 6D).

#### **Fault Kinematics**

Slickenline lineation orientations from brittle damage zones yield kinematics for faults in the McCallum Creek area. Contouring the surface trace of the McCallum Creek fault on the geologic map shows the western section of the McCallum Creek fault strikes ~340 and dips ~70°NE. The measured fault-plane solutions for the western section of the fault (locales 14ATW-42 and 17ATW-16) show a NW-striking dextral fault that dips steeply to the southwest or northeast (Fig. 8A). Measured fault-plane solutions for the eastern section of the McCallum Creek fault (locales 14ATW-23 and 14ATW-02) show thrust kinematics on a fault oriented similar to the attitude of ~285/35°N measured from the geologic map. Fault-plane solutions from slickenline lineations in the damage zone of the Hoodoo fault, north of the McCallum Creek fault, generally indicate dextral kinematics (Waldien, 2015).

Both the measured and predicted fault-plane solutions are consistent with NNE-SSW convergence on the McCallum Creek fault (Fig. 8A). Ratchkovski et al. (2004) present stress-tensor inversions from two sets of earthquake data from the region of the 2002 M<sub>w</sub> 7.9 Denali earthquake rupture through the Alaska Range. One stress-tensor inversion uses aftershock seismicity from the 2002 Denali earthquake, which reveals a subhorizontal maximum principal stress (o<sub>1</sub>) trending ~195-015 in the McCallum Creek area (Fig. 8B). A second stress-tensor inversion uses earthquake data collected over the 30 years prior to the 2002 Denali earthquake and yields a similarly subhorizontal maximum principal stress axis trending ~185-005 in the McCallum Creek area (Fig. 8B). These stress-tensor inversions suggest that the shortening axis recorded by aftershocks from the 2002 Denali earthquake on the section of the rupture adjacent to the McCallum Creek fault match the shortening axis recorded by background seismicity, even though the inversions show a ~90° rotation of the minimum ( $\sigma_3$ ) and intermediate ( $\sigma_2$ ) principal stress axes about an axis approximately parallel to the maximum principal stress ( $\sigma_1$ ) (Ratchkovski et al., 2004) (Fig. 8B). Interpreting these principal stress orientations as principal strain rate axes (e.g., Twiss and Unruh, 1998) implies that the NNE-SSW-oriented convergence for the McCallum Creek fault indicated by measured fault-plane solutions is consistent with the stress-tensor inversions.

The orientation of the McCallum Creek fault plane determined by measured fault-plane solutions is similar to the fault orientation measured from the geologic map. The dextral kinematics and variable dip direction on the western section of the McCallum Creek fault indicated by the measured fault-plane solutions differ slightly from the dextral-reverse slip and northeast dip of the fault produced by the predicted fault-plane solutions (Fig. 8). The thrust kinematics and moderate north dip on the eastern section of the McCallum

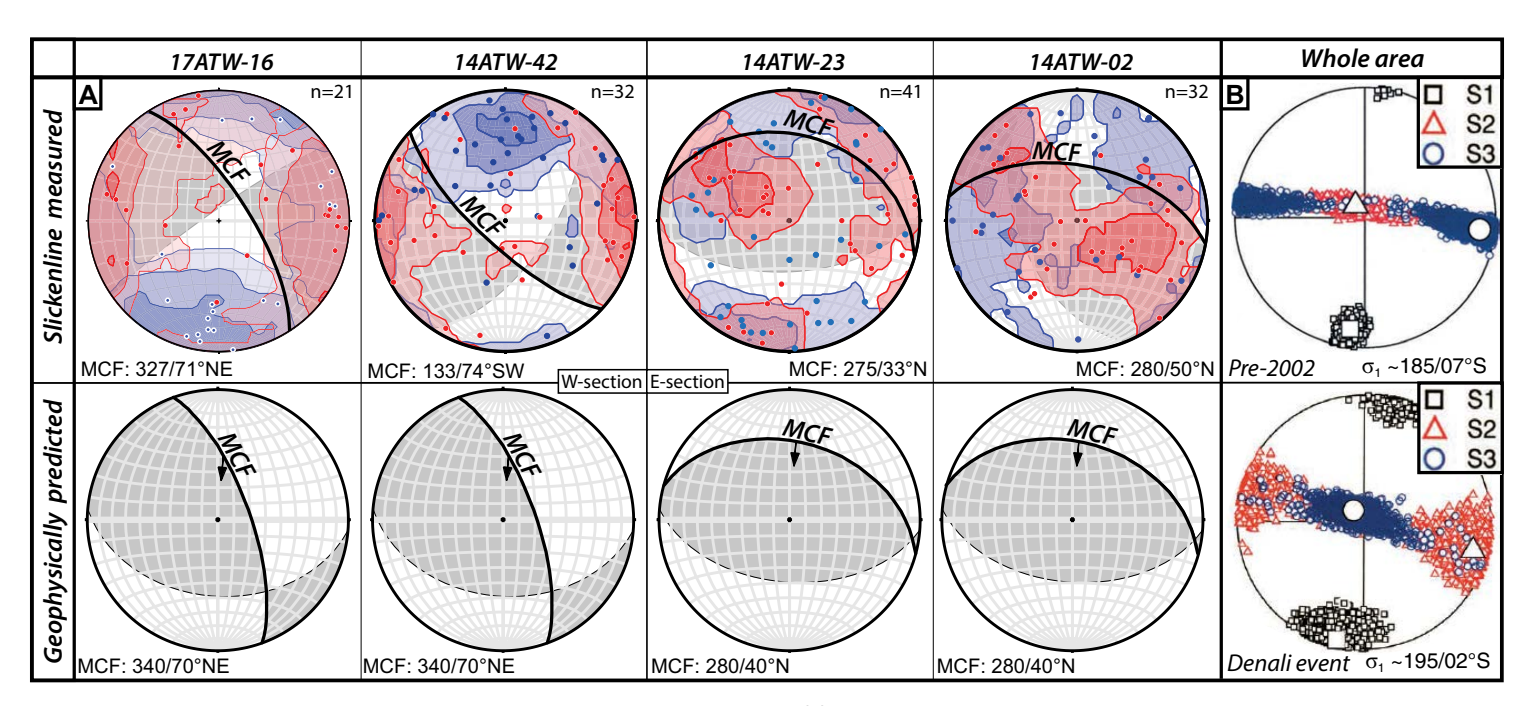


Figure 8. Lower hemisphere Schmidt projections showing the kinematics of the McCallum Creek fault. (A) Fault-plane solutions for the McCallum Creek fault constructed from measured slickenline lineation data (top) and predicted using the orientation of the McCallum Creek fault from the geologic map (Plate 1) and geophysically determined principal stress axes (bottom). Red and blue points in the measured fault-plane solutions represent the tension and compression axes for each fault plane measurement, respectively. Red and blue zones are 2σ contour intervals of tension axes and compression axes, respectively, wherein lighter shades represent higher levels of uncertainty. Gray quadrants are intersected by the average tension axis, and white quadrants are intersected by the average compression axis. The number (n) of fault plane measurements for each fault-plane solution is given. The nodal plane interpreted to represent the McCallum Creek fault (MCF) is bold and labeled. The arrow on the predicted fault-plane solutions is the hanging wall transport direction inferred from stress-tensor inversions (Ratchkovski et al., 2004). (B) (Top) stress-tensor inversions from Ratchkovski et al. (2004) showing principal stress (strain rate) axes for earthquakes prior to the 2002 Denali earthquake: σ<sub>1</sub>—black squares; σ<sub>2</sub>—blue circles; σ<sub>3</sub>—red triangles. The average maximum principal stress (σ<sub>1</sub>) is oriented ~185/02°S. Note that the intermediate and minimum principal stress axes rotate between the two time frames.

Creek fault indicated by the measured fault-plane solutions are consistent with kinematics of the McCallum Creek fault produced by the predicted fault-plane solutions (Fig. 8).

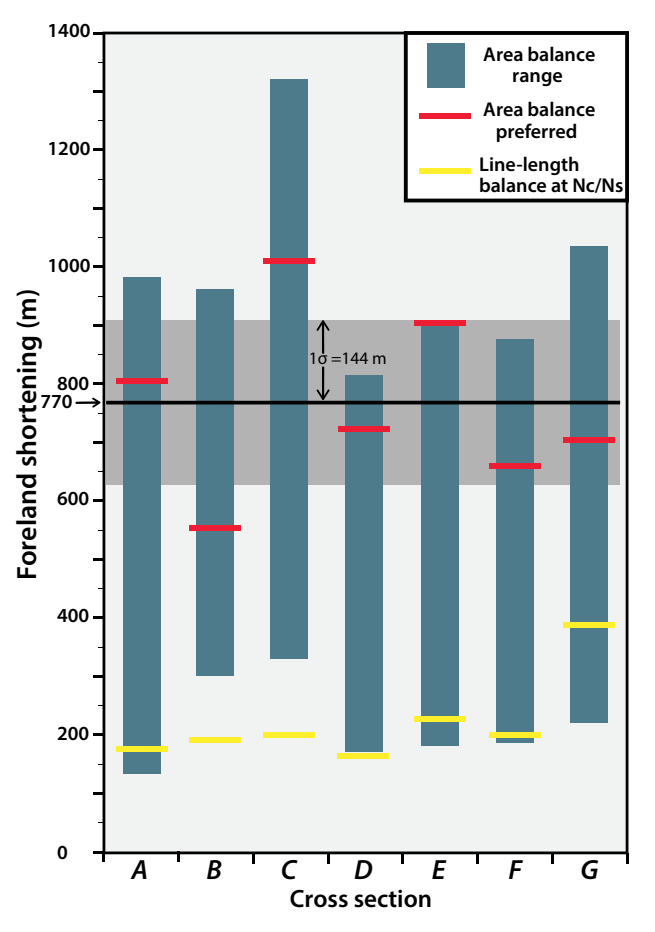
# **Balanced Cross Sections**

Folding of the McCallum Formation provides a record that shortening was transferred from the main McCallum Creek fault into the foreland basin. The variability in fold shape and presence of tear faults described above require a suite of cross sections to show the structure of the foreland thrust system. Accordingly, we produced seven forward kinematic balanced cross section models through the foreland thrust system (cross sections A–G; Fig. 5 and Plate 1). Due to uncertainties in the geometry of the blind foreland thrust system and thickness of McCallum Formation strata involved in the deformation, we ad-

justed model parameters related to these variables between model iterations. The modeling process results in a range of shortening values for each cross section and allows for an estimate of total shortening throughout the foreland thrust system (Fig. 9).

Estimates for total shortening in the McCallum foreland thrust system vary with balancing technique. Line-length shortening values are sensitive to limb dip and stratigraphic position; therefore this method shows more shortening on folds with steeply dipping limbs (e.g., cross section G; Fig. 9). Shortening values produced by the area balancing technique are less sensitive to limb dip but may change drastically with the geometry of the initial stratigraphic wedge (Judge and Allmendinger, 2011). In the case of the McCallum Formation, the thickness and depositional taper of the upper member is the primary control on the shape of the initial stratigraphic wedge. Poor exposure in many areas of the McCallum foreland generates uncertainty in the thickness of the upper McCallum Formation, which may also vary along strike of the McCallum Creek

Figure 9. Range in modeled shortening values for the foreland thrust system. Teal bars represent the variability in area shortening values that result from varying the décollement location and initial stratigraphic taper in viable models. Yellow bars are line-length shortening values for each preferred cross section measured at the contact between the upper and lower Mc-Callum Formation (Nc/Ns). Red bars are area balanced shortening values for each preferred cross section model (Plate 1). The dark gray line at 770 m is the average of all area balanced preferred cross sections (red bars). Lighter gray zone around the average preferred shortening value is the 1<sub>o</sub> uncertainty on the average preferred shortening value. Supplemental File S2 (see text footnote 1) contains the data represented by the graph.



fault. As a rudimentary treatment of these issues, we incorporated variations in thickness and stratigraphic taper of the upper McCallum Formation into the cross section models. For a given depth to décollement, cross sections constructed with a thinner upper McCallum Formation and/or more taper toward the foreland (thicker in north) result in more shortening. Holding all other variables constant, cross sections constructed with a thicker upper McCallum Formation and/or little stratigraphic taper (tabular shape) yield lower shortening values. For a given stratigraphic thickness and taper, the location of the basal décollement controls the thickness of strata involved in the deformation and therefore must also be determined to accurately calculate the total foreland shortening using the area balancing technique.

Surface geologic data and subsurface geophysical data in the McCallum foreland could fit a range of possible décollement locations. Seismic reflection suggests the lower member of the McCallum Formation is ~1000 m thick and unconformably overlays Wrangellia rocks (Brocher et al., 2004). Only ~100 m of the lower member are exposed in the field area (Allen et al., 2014), and all thrusts in the foreland thrust system are blind (Fig. 5; Plate 1). These observations and the low competency of the lower member lacustrine strata bracket the location of the décollement to the lower ~900 m of the McCallum Formation. The range of area-shortening values in Figure 9 results from uncertainties locating the décollement in the lower 900 m of the lower McCallum Formation using only surface geologic data. Each preferred balanced cross section model in the foreland thrust system yields a décollement between 200 and 400 m above sea level (550-750 m below the alluvial plain of Phelan Creek), resulting in a mean basin-wide shortening estimate of 770 ± 144 m (1σ) (Fig. 9; Table S2-1 [footnote 1]). Plotting poles to bedding in the foreland fold trains records shortening along azimuth ~004-184 (Fig. 7).

# **Apatite Fission-Track Thermochronology**

Five of our six bedrock AFT samples (14ATW-45, 14ATW-50, 14ATW-52, 01CAN, and 81COL) in the hanging wall of the McCallum Creek fault record the onset of rapid cooling through the AFT partial annealing zone near the Miocene-Pliocene boundary (Table 1). The narrow range of track lengths, which cluster around 14 µm, indicate cooling was rapid (Fig. 10). 40 Ar/39 Ar K-feldspar minimum ages on two samples (81COL and 60COL; Fig. 3) from the plutonic complex in the hanging wall of the McCallum Creek fault indicate these rocks cooled through ~150 °C at ca. 81-105 Ma (Benowitz et al., 2014). HeFTy thermal modeling of samples 14ATW-45, 14ATW-50, 14ATW-52, 01CAN, and 81COL using 40Ar/39Ar K-feldspar minimum ages as high(er) temperature inputs show the onset of rapid cooling from ~150-135 °C to the surface between ca. 5-8 Ma (Table 2). One sample (07JB59) ~3.5 km east of 14ATW-50 shows cooling through AHe closure at ca. 4 Ma (Perry, 2014), concordant with the Pliocene-Quaternary rapid cooling trend suggested by the HeFTy thermal models (Figs. 3 and 10).

In the southwestern corner of the hanging wall, sample 14ATW-34B records AFT closure at 33 ± 5.4 Ma. The narrow range of fission-track lengths with a mean of ~14 µm indicates the sample passed rapidly through the partial annealing zone. Thermal modeling for this sample shows the onset of rapid cooling at ca. 35-40 Ma (Fig. 10). Apatite fission-track cooling ages near the College glacier and east of the study area also preserve a phase of Oligocene-early Miocene cooling (Perry, 2014).

Independent of young cooling ages in the hanging wall of the McCallum Creek fault, we observe that: (1) the surface trace of the McCallum Creek fault coincides with a steep topographic gradient; (2) the McCallum Creek fault thrusts pre-Neogene strata over late Miocene-Pliocene strata (McCallum Formation); (3) the McCallum Formation contains an abrupt facies transition near the Miocene-Pliocene boundary; (4) the upper McCallum Formation contains clasts sourced in part from the hanging wall of the McCallum Creek fault; and

TABLE 1. APATITE FISSION-TRACK ANALYTICAL RESULTS

Sample	No. grains*	Mean U (ppm)	χ² probability (%)	Fission-track age [1σ] (Ma)	Mean track length [1σ] (μm)	No. tracks†	Mean Dpar (μm)	Latitude (°N)	Longitude (°W)	Elevation (m)	Rock type
81COL	40	24.0	51.0	4.6 [0.6]	14.66 [1.03]	61.0	2.63	63.2706	145.2977	2383	Granitoid
01CAN	40	1.6	22.6	5.1 [2.1]	14.68 [0.99]	20.0	1.39	63.3369	145.6084	1150	Granitoid
14ATW-34B	34	8.8	0.0	33. [5.4]	14.03 [1.32]	71.0	2.05	63.2643	145.623	1214	Meta-andesite
14ATW-45	35	47.9	0.0	6.7 [3.6]	13.75 [1.67]	63.0	2.03	63.2321	145.5566	1412	Meta-andesite
14ATW-50	39	3.6	18.0	6.5 [2.4]	14.34 [1.76]	30.0	1.70	63.2483	145.4094	1751	Granitoid
14ATW-52	36	3.07	0.0	5.9 [2.4]	13.85 [1.32]	6.0	1.73	63.2675	145.4022	1640	Granitoid

<sup>\*</sup>Grains used to calculate pooled age and perform thermal modeling.

(5) McCallum Formation strata are folded, with fold axes subparallel to the trace of the McCallum Creek fault. These observations require significant late Miocene-Pliocene shortening on the McCallum Creek fault and foreland structures, which would result in uplift and erosion of rocks above the McCallum Creek fault ramp and deposition into the subjacent foreland basin. Because the timing of rapid cooling in the hanging wall overlaps with deposition and the facies transition in the foreland basin strata, we interpret late Miocene-Pliocene rapid cooling in the area to reflect rock uplift and exhumation due to the vertical component of slip on the N-dipping McCallum Creek fault.

The timing and amount of exhumation for samples in the hanging wall of the McCallum Creek fault may be estimated from the location of the inflection point between the slow cooling and rapid cooling domains in HeFTy thermal models and inferences about the paleogeothermal gradient. The locations of inflection points for "good" (GOF >0.5; purple zones in Fig. 10) model iterations on samples 14ATW-45, 14ATW-50, 14ATW-52, 01CAN, and 81COL range between ca. 10-5 Ma and ~190-110 °C (Table 2). Averaging the location of the inflection point on the best-fit model curve for these samples gives the onset of rapid cooling from ~145 °C at ca. 7 Ma. Heat flow information (Batir et al., 2013) and thermal conductivity (Eppelbaum et al., 2014) of rock types from the McCallum Creek area yield a modern geothermal gradient between 30 and 37 °C/km. Other low-temperature thermochronology studies in the eastern Alaska Range (e.g., Benowitz et al., 2014) use a paleogeothermal gradient of 30 °C/km to estimate total Cenozoic exhumation. Applying a paleogeothermal gradient of 30 °C/km and a mean annual surface temperature of 0 °C since the early Pliocene (cf. Ager, 2007) to the averaged temperatures at the bestfit model curve inflection points for these five samples results in ~4.8 km of exhumation since the initiation of rapid rock cooling at ca. 7 Ma. The pooled AFT ages and long track lengths for samples 14ATW-45, 14ATW-50, 14ATW-52, 01CAN, and 81COL suggest rapid cooling through the partial annealing zone was under way by ca. 6 Ma. Inferring exhumation from ~4.8 km depth, stationary isothermal surfaces, a stable geothermal gradient, and a constant cooling rate, these five samples have been exhumed ~4.1 km since they passed through AFT closure at ca. 6 Ma (Fig. 11).

#### DISCUSSION

# **Linked Neogene Exhumation and Basin Development** in the McCallum Creek Area

Apatite fission-track cooling ages from the hanging wall of the McCallum Creek fault primarily show rapid cooling during the late Miocene and through the Pliocene. Thermal models of AFT and 40Ar/39Ar K-feldspar ages show that most samples in the hanging wall of the McCallum Creek fault transitioned from slow cooling to rapid cooling at ca. 7 Ma (Fig. 10). Although the base of the lower McCallum Formation is not exposed, 40Ar/39Ar ages from exposed ash beds in the lower McCallum Formation indicate that the foreland basin initiated prior to ca. 6 Ma (Kunk, 1995; Benowitz et al., 2007). The abrupt facies transition marking the onset of upper McCallum Formation conglomerates occurred shortly before ca. 5 Ma (Allen, 2016). Because both members of the McCallum Formation are cut by the McCallum Creek fault, we interpret the facies transition to record the hanging wall of the fault overriding the lower McCallum Formation and shifting the proximal depositional environment farther south into the foreland. Taken together, we interpret these observations to reflect a genetic linkage between slip on the McCallum Creek fault, erosion of hanging wall rocks, and deposition into the foreland basin.

In addition to the record of late Miocene-Pliocene unroofing and faulting, hanging wall rocks also record a phase of late Eocene-Oligocene cooling. The thermal model for sample 14ATW-34B shows rapid cooling starting at ca. 40 Ma, passage through AFT closure at ca. 33 Ma, and continued cooling throughout the Neogene (Fig. 10). Although there is regional magmatism in the late Eocene (Benowitz et al., 2011), igneous rocks of the appropriate age are apparently absent from the McCallum Creek area. There is, however, evidence for regional faulting in the mid-Cenozoic, which may have influenced cooling in the McCallum Creek area. To the west, early Oligocene cooling throughout the eastern Alaska Range and Amphitheater Mountains has been interpreted to record slip on the Broxson Gulch fault and related structures (Turner and Smith, 1974; Benowitz et al., 2017; Waldien et al., 2017). Because sample 14ATW-34B is

<sup>†</sup>Tracks are spontaneous tracks.

Dpar—the arithmetic mean fission-track etch figure diameter parallel to the crystallographic c-axis.

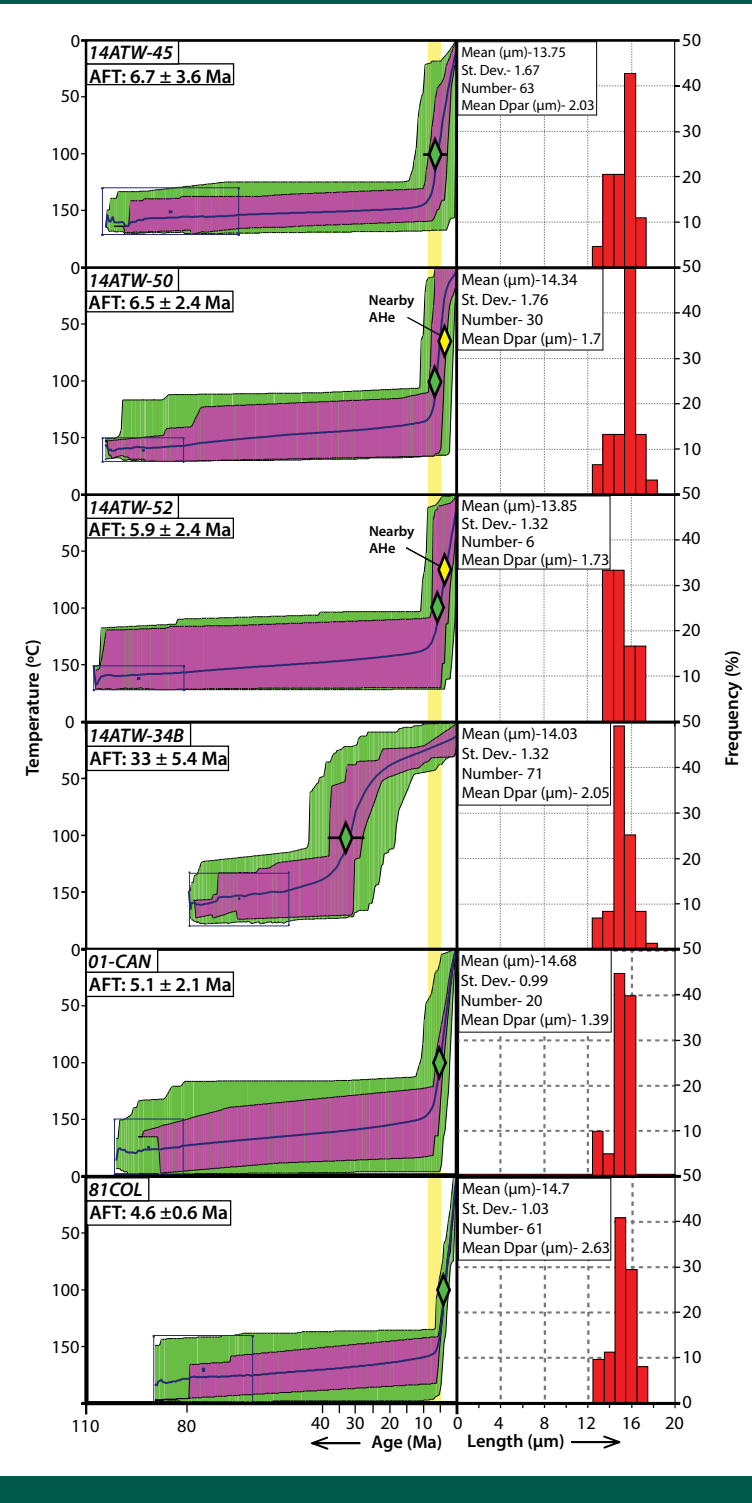


Figure 10. Apatite fission-track (AFT) time-temperature model data outputs from HeFTy. Sample numbers and pooled ages with 1 $\sigma$  uncertainties are given. The purple area in time-temperature plots encompasses model iterations with a goodness of fit >0.5, and the green area encompasses model iterations with a goodness of fit >0.05 after 20,000 model iterations using the annealing model of Ketcham et al. (1999) and c-axis projection of Donelick et al. (1999). Goodness of fit criteria are outlined in Ketcham (2005).  $^{40}$ Ar/ $^{39}$ Ar K-feldspar ages from Benowitz et al. (2014) are used as high-temperature (≥150°C) constraints (samples 81COL and 60COL, Fig. 3). The blue line is the weighted mean cooling path determined by HeFTy. Green diamonds represent the pooled AFT age for each sample. Yellow diamonds on models 14ATW-50 and 14ATW-52 represent an AHe age from Perry (2014), ~3.5 km east of these samples (Fig. 3). Yellow bar in the background highlights the regional increase in rock cooling rate at ca. 8–5 Ma. Histograms show fission-track length distributions and track statistics for each sample.

near these structures, the ca. 33 Ma AFT age may also be related to deformation associated with the Broxson Gulch thrust system. Alternatively, the Oligocene cooling may record slip on the Hoodoo fault, which cuts Eocene volcanic strata in the hanging wall of the McCallum Creek fault and is also cut by the western section of the McCallum Creek fault (Fig. 5; Plate 1). Fault kinematic measurements from the Hoodoo fault damage zone potentially record multiple phases of slip on the fault but nonetheless show a component of north-side-up separation in addition to lateral slip (Waldien, 2015). Because the Hoodoo fault was active between ca. 50–6 Ma and sample 14ATW-34B is in the upthrown side of the fault, it is possible that slip on the Hoodoo fault facilitated Oligocene cooling in the area. At the eastern margin of the study area, AFT cooling ages on the arête east of the College glacier also record passage through AFT closure in the Oligocene and Miocene (ca. 29–21 Ma) (Perry, 2014). Because other samples within ~4 km do not record this mid-Cenozoic cooling (Figs. 3 and 10), we hypothesize that a fault presently buried beneath the College glacier caused

TABLE 2. HeFTy INFLECTION POINTS USED TO ESTIMATE TOTAL EXHUMATION

Sample	Location of inflection point on model	Time (m.y.)	Temperature (°C)		
14TW-45	Тор	10	130		
	Bottom	7	160		
	Best fit	8	145		
14TW-50	Тор	8	110		
	Bottom	6	165		
	Best fit	8	135		
14TW-52	Тор	8	110		
	Bottom	5	170		
	Best fit	8	135		
01CAN	Тор	8	130		
	Bottom	6	190		
	Best fit	8	150		
81COL	Тор	5	150		
	Bottom	6	180		
	Best fit	6	150		
Average		7.13	147.33		

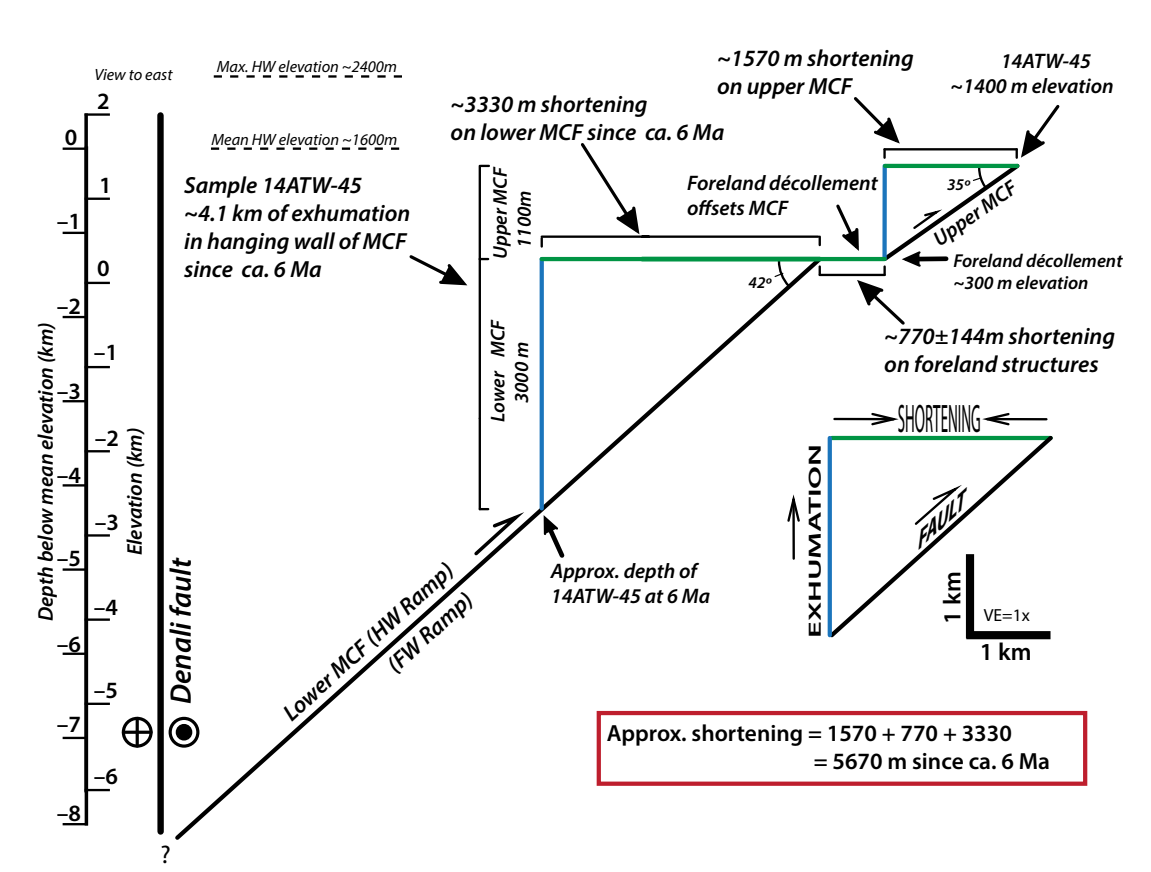


Figure 11. Geometric model of exhumation (blue lines) and shortening (green lines) due to slip on the McCallum Creek thrust system, using sample 14ATW-45 as a marker. Dip of the upper McCallum Creek fault (MCF) is based on the geologic map and kinematics data. Dip of the lower Mc-Callum Creek fault is based on earthquake hypocenter locations from Ratchkovski et al. (2003, 2004) averaged to 42°. The total exhumation estimate assumes a stationary geothermal gradient of 30 °C/km. The shortening estimate on the upper Mc-Callum Creek fault is calculated using the fault dip and the elevation difference between the foreland décollement and sample 14ATW-45. Shortening since apatite fission-track closure at ca. 6 Ma estimated for the entire thrust system is calculated using fault dip, ~4.1 km of total exhumation experienced by sample 14ATW-45. and ~770 m of shortening in the foreland thrust system. FW-footwall: HW-hanging wall; VE-vertical exaggeration.

rocks on either side to experience distinct late Cenozoic cooling histories. This hypothesized fault would strike ~NNE and would have experienced a phase of Oligocene–early Miocene east-side-up displacement. Apatite (U-Th)/He cooling ages from the same samples on the arête east of the College glacier record cooling through ~70 °C during the Pliocene. These ages align with modeled cooling paths of the ca. 6 Ma AFT ages (Fig. 10). Therefore, on the basis of the older AFT cooling ages, we infer that Oligocene–early Miocene faulting in the hanging wall of the present McCallum Creek fault may have offset the AFT partial annealing zone in some locations, but all hanging wall rocks in the area experienced a similar cooling path during the Pliocene and Quaternary.

# Late Miocene–Quaternary Shortening on the McCallum Creek Fault

Fault kinematics measurements from both the eastern and western sections of the McCallum Creek fault record ~NNE-SSW shortening and are compatible with stress-tensor inversions from historic seismicity. Measured fault-

plane solutions at locales 14ATW-23 and 14ATW-02 along the eastern section of the fault record reverse slip on a moderately N-dipping fault, which is consistent with the predicted fault-plane solutions and the map pattern along this section of the fault (Figs. 5 and 8; Plate 1). The measured fault-plane solutions at locales 17ATW-16 and 14ATW-42 from the western section of the fault show predominantly dextral slip and a McCallum Creek fault plane that may dip southwest rather than northeast as indicated by the geologic map (Figs. 5 and 8; Plate 1). One interpretation of these data could be that the western section of the McCallum Creek fault is an inherited dextral fault that has been reactivated during the Neogene. This interpretation implies that at least some of the slickenlines in the modern damage zone formed during a previous phase of slip on the fault. However, the tension and compression axes cluster reasonably well for locales along the western section of the fault. As a result of the tightly clustered data set, multiple sets of nodal planes could satisfy the fault-plane solution if the shear zone symmetry is reduced beyond orthorhombic (Twiss and Unruh, 1998). Low symmetry in brittle shear zones may result from rotation of blocks within the fault zone, preferred slip planes, or combined coaxial and non-coaxial deformation (Twiss and Unruh, 1998). Because these features are common in brittle shear zones and not addressed in our analysis of the McCallum Creek fault, we consider the measured and predicted fault-plane solutions for the western section of the McCallum Creek fault to be internally consistent and record dextral-thrust oblique slip on a steeply NE-dipping fault. This interpretation does not preclude the possibility that the late Miocene—Quaternary McCallum Creek fault is a reactivated structure, but it does enforce the conclusion that the McCallum Creek fault has accommodated shortening at an angle nearly perpendicular to the Denali fault since at least the late Miocene.

The along-strike change in kinematics on the McCallum Creek fault is also recorded in the AFT cooling ages and the distribution of foreland basin strata. The change in strike between the eastern and western sections of the fault is accompanied by a change from thrust to oblique kinematics. Therefore, the fault kinematics record relative motion between the hanging wall and footwall blocks that is uniform along strike of the McCallum Creek fault. Because the western section of the fault has a considerable strike-slip component, the potential for lower erosion rates during hanging wall rock uplift may have preserved the ca. 33 Ma AFT cooling age in sample 14ATW-34B. Basin development in the footwall of the eastern section and a lack of preserved Neogene strata in the footwall of the western section of the fault further support a change from reverse to oblique-slip kinematics.

Agreement between fault kinematics on the eastern McCallum Creek fault and the shortening direction in the folded foreland strata shows that contraction in the McCallum Creek thrust system is oriented along azimuth ~005–185 (Figs. 7 and 8). Inferring that the brittle slickenline lineations preserved in the McCallum Creek fault damage zone formed continuously over the duration of slip on the McCallum Creek fault, the tension and compression axes in the measured fault-plane solutions suggest the convergence direction on the south side of the Denali fault in the McCallum Creek area has remained consistent since the phase of late Miocene thrusting on the McCallum Creek fault began. Restoring slip on the eastern Denali and Totschunda faults at their current rates (Haeussler et al., 2017b) for 7 m.y. places the field area (Fig. 3) a maximum of ~91 km to the southeast of its current location. The modern Denali fault changes strike by only ~5° over this distance (Fig. 2).

Assuming that neither the central Denali, Totschunda, nor McCallum Creek faults have drastically changed strike in the past 6–7 m.y. and that the relative plate motion vector has remained constant, the convergence direction on the McCallum Creek fault would remain essentially constant as it is translated along the south side of the Denali fault. Given that the kinematics of the McCallum Creek thrust system, the Denali fault, and other regional thrust faults to the north collectively record slip partitioning of transpressional deformation over the past 6–7 m.y., we infer the above assumptions are valid and that the current structural geometry has accommodated long-term oblique plate motion as a set of partitioned dextral and convergent structures.

The rupture dynamics of the 2002  $M_{\rm w}$  7.9 Denali earthquake also indicate that modern deformation associated with the McCallum Creek fault has been

consistent from late Miocene until the present. Low-temperature thermochronology studies in the eastern Alaska Range northwest of the McCallum Creek area show that rapid Neogene-Quaternary cooling is spatially coincident with topography on the north side of the Denali fault (Benowitz et al., 2011, 2014; Perry, 2014) (Fig. 2). Rapid cooling and high topography in that region are consistent with the north-side-up vertical component of slip on that section of the 2002 rupture. The section of the Denali fault beneath the Canwell glacier north of the McCallum Creek area is the only significant section along the 2002 Denali rupture to show south-side-up vertical slip in addition to dextral slip (Haeussler et al., 2004). Post-late Miocene rapid cooling in the hanging wall of the McCallum Creek fault and south-side-up vertical slip on the Canwell glacier section of the Denali fault rupture suggest that the entire hanging wall of the McCallum Creek fault has been moving vertically as a relatively coherent block while synchronously being translated along the Denali fault. Exhumation of a coherent wedge-shaped block between the subvertical Denali fault and moderately dipping McCallum Creek fault throughout the Pliocene further advocates that thrust kinematics shown by the measured fault-plane solutions represent a long-lived (~5–7 m.y.) record of convergence on the fault. The hanging wall cooling ages and fault kinematics data presented here also support the alignment of earthquake hypocenters showing that the McCallum Creek fault is a moderately dipping planar feature that links to the Denali fault at depth (Brocher et al., 2004) (Fig. 4). Although the surface trace of the McCallum Creek fault appears to lack fault scarps, the historic seismicity indicates that the structure is active at depth and may transfer slip into the foreland thrust system.

# **Development and Dynamics of the McCallum Creek Thrust System**

#### Kinematic Evolution of Shortening Structures

During translation along the Denali fault, the McCallum Creek thrust system developed by slip on both the McCallum Creek fault and the kinematically linked foreland blind thrust faults (Fig. 12). Combining the shortening direction determined from bedding attitude measurements in the foreland fold trains with kinematics from the measured and predicted fault-plane solutions shows that the convergence directions independently recorded in the seismicity, foreland thrust system, and McCallum Creek fault damage zone are coincident (Figs. 7 and 8). We interpret this observation to reflect a kinematic linkage between the main McCallum Creek fault and the blind foreland thrusts and a uniform shortening direction throughout the various stages of thrust system development.

The late Miocene–Pliocene foreland basin stratigraphy records a switch from slip on the main McCallum Creek fault to the imbricate foreland thrust system. Propagation of the deformation front into the foreland basin strata likely resulted in basin inversion involving some combination of: (1) incision of the paleodrainage network into the foreland strata; (2) development of an axial drainage system parallel to the thrust front; and (3) sediment deposition on the limbs of growing folds (growth strata). Since the 315 m of stratigraphy

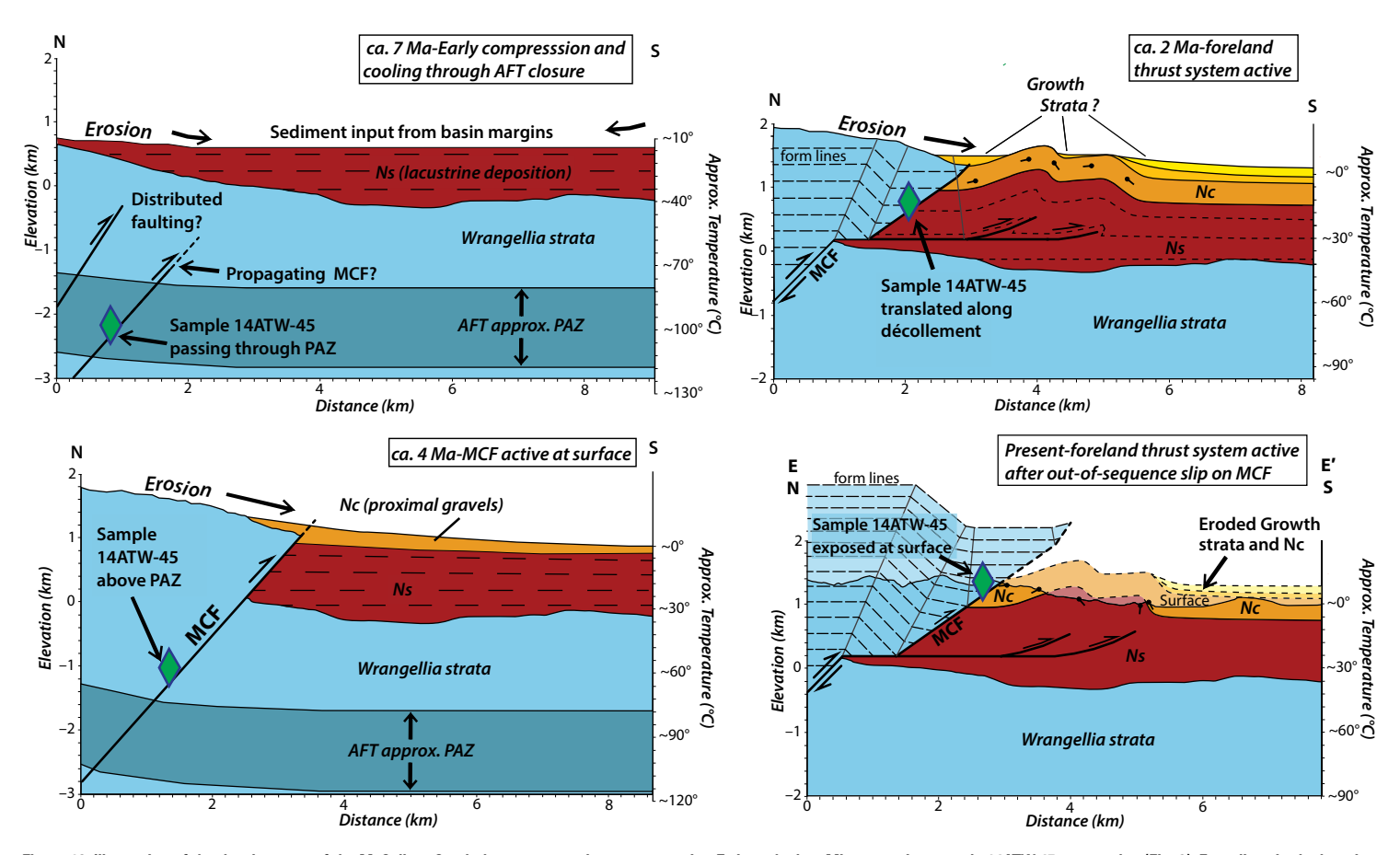


Figure 12. Illustration of the development of the McCallum Creek thrust system along cross section E since the late Miocene using sample 14ATW-45 as a marker (Fig. 3). Form lines in the hanging wall of the McCallum Creek fault (MCF) in the last two frames are intended to illustrate folding of hanging wall rocks due to development of the foreland décollement and out-of-sequence slip on the main McCallum Creek fault. The "Present" configuration of cross section E shows the upper and lower segments of the McCallum Creek fault are offset by 770 m on the basis of average shortening in the foreland thrust system. Pastel colors above the surface in the "Present" frame represent material that has been eroded. See the legend in Plate 1 for unit labels. PAZ – AFT (apatite fission-track) partial annealing zone.

measured in the McCallum Formation in the field area lack fanning angular unconformities, which would indicate growth strata, and all observed paleoflow indicators in the upper McCallum Formation show approximately S-directed flow (Allen, 2016), we interpret that the foreland thrust system developed after ~215 m of the upper McCallum Formation were deposited. The ca. 3.8 Ma tephra at 200 m above the base of the upper McCallum Formation places an upper age constraint on the initiation of the foreland thrust system (Fig. 5; Plate 1). Subsequent dissection of the foreland strata likely eroded a stratigraphically higher portion of the upper McCallum Formation and deposited detritus in localized topographic depressions on the limbs of folds (Fig. 12). The ~6°N dip of the

Plio-Pleistocene glacial deposit (map unit QNog) suggests it was deposited in such a setting on the backlimb of the fold in cross section F (Plate 1).

Field and map evidence suggests that slip in the McCallum Creek thrust system has alternated between the main McCallum Creek fault and the foreland thrust system since mid-Pliocene development of the foreland thrust system. Following late Miocene thrusting on the main McCallum Creek fault, shortening in the foreland thrust system caused the portion of the McCallum Creek fault above the foreland décollement to be separated from the portion below the décollement, resulting in division of the McCallum Creek fault into upper and lower segments (Figs. 11 and 12). Evidence for out-of-sequence slip

on the main McCallum Creek fault includes: (1) the upper McCallum Creek fault bounds a thinned portion of the upper McCallum Formation in the north limb of the fold in cross section G (Plate 1); (2) N-dipping strata of the McCallum Formation are cataclastized along bedding planes, which dip subparallel to the upper McCallum Creek fault; and (3) the upper McCallum Creek fault crosscuts fold axes in the foreland thrust system (Plate 1). Development of folds structurally beneath the upper McCallum Creek fault would fold the fault plane. On the N-dipping backlimb of a foreland fold, the section of the upper McCallum Creek fault that has been translated onto the foreland ramp would increase in dip by a value equal to dip of the foreland thrust ramp, giving the upper McCallum Creek fault a listric shape (Fig. 12; 2 Ma panel). Where exposed, the surface trace of the upper McCallum Creek fault has generally planar morphology and truncates N-dipping fold limbs related to the foreland thrust system (Plate 1). This relationship indicates that out-of-sequence slip on the main McCallum Creek fault caused the folded listric portion of the upper McCallum Creek fault to be eroded away, exposing a lower unfolded portion of the fault (Fig. 12).

One location where the surface exposure of the McCallum Creek fault is not planar is near cross section G. In this location, the McCallum Creek fault decreases dip across the axis of the fold in cross section G. Growth of a fold structurally beneath the McCallum Creek fault will cause the portion of the fault above the S-dipping fold limb to rotate toward the south. Such rotation would have the effect of decreasing the northward dip of the McCallum Creek fault above the southern fold limb. The observed magnitude of dip reduction (~15°) is too small to have the McCallum Creek fault folded during the entire development of foreland fold G because the forelimb of the fold dips ~30°S. Therefore, we interpret this structural relationship to record alternating slip between the main McCallum Creek fault and the foreland thrust system. The map distance between the structurally thinned strata in the northern fold limb in cross section G and the southern extent of the McCallum Creek fault is ~1350 m. We interpret this distance to be the shortening component of out-of-sequence slip on the main McCallum Creek fault. Our age of ca. 3.8 Ma to bracket the initiation of the foreland thrust system requires that the out-of-sequence slip would have occurred since the mid-Pliocene.

Incision of the modern drainage network into the foreland, local stream segment incision, perched fluvial terraces across fold limbs, and tilted glacial outwash strata suggest that foreland structures are the active part of the McCallum Creek thrust system (Waldien, 2015) (Figs. 6C and 6D). Aftershock seismicity from the 2002 Denali earthquake as shallow as the approximate location of the foreland décollement also suggests that slip from the lower McCallum Creek fault is distributed into the weak and potentially aseismic foreland strata rather than the upper McCallum Creek fault (Fig. 4). Although beyond the scope of this paper, a detailed investigation of the Quaternary stratigraphy and tectonic geomorphology in the McCallum foreland would likely yield fruitful results describing the Quaternary activity of the McCallum Creek thrust system to better characterize the thrust fault-related seismic hazard in the region.

The magnitude of late Miocene–Quaternary shortening on the McCallum Creek thrust system can be calculated by summing shortening documented

on the foreland thrust system, the upper McCallum Creek fault, and the lower McCallum Creek fault (Fig. 11). The location of sample 14ATW-45 near the surface trace of the McCallum Creek fault makes it a good marker to reconstruct the exhumation and shortening history for the thrust system (Figs. 3, 11, and 12). Following the precedent set by other low-temperature thermochronology studies in the eastern Alaska Range (e.g., Benowitz et al., 2011, 2014), we infer a paleogeothermal gradient of 30 °C/km, which results in ~4.1 km of rock uplift and related exhumation since sample 14ATW-45 passed through the AFT closure isotherm at ca. 6 Ma. Assuming a constant geothermal gradient that is stationary relative to the McCallum Creek fault blocks, shortening magnitudes for both the upper and lower segments of the McCallum Creek fault can be calculated using fault dip from geophysical information and mapping, the location of the foreland décollement from balanced cross sections, and the total exhumation estimate from AFT cooling ages. Our geologic mapping and measured fault-plane solutions show the upper McCallum Creek fault dips ~35°N (Fig. 8; Plate 1). Approximately 1.1 km of rock uplift and exhumation on the upper McCallum Creek fault above the foreland décollement result in ~1.57 km of shortening (Fig. 11). The lower McCallum Creek fault accommodated the remaining ~3 km of rock uplift and exhumation. Aftershock hypocenter locations suggest the dip of the lower McCallum Creek fault is between 40° and 45°. Averaging the dip to 42° yields ~3.33 km of shortening from ~3 km of exhumation on that segment of the fault (Fig. 11). Summing the shortening values from the upper and lower segments of the McCallum Creek fault with 770 ± 144 m of shortening accommodated by the blind foreland thrusts results in ~5.7 km of total shortening for the entire McCallum Creek thrust system since sample 14ATW-45 cooled below AFT closure at ca. 6 Ma (Fig. 11). The thermochronology data do not record the time that 14ATW-45 was being translated along the foreland décollement or out-of-sequence slip on the upper McCallum Creek fault because 14ATW-45 had already passed through AFT closure before the foreland thrust system developed (Fig. 12). Aside from 14ATW-45 (AFT ca. 6 Ma) and 14ATW34B (AFT ca. 33 Ma), all samples with AFT ages presented here are presently above the lower McCallum Creek fault ramp and therefore only record shortening and exhumation resulting from slip on this segment of the fault. Widespread ca. 6 Ma cooling in the hanging wall of the McCallum Creek fault suggests that hanging wall samples passed through the AFT closure isotherm while located above the lower McCallum Creek fault ramp. This further supports our inference that the foreland décollement is located in the lower McCallum Formation above the AFT closure isotherm (Fig. 12).

Calculating a shortening rate since ca. 6 Ma for the McCallum Creek thrust system would be misleading due to assumptions made in the total shortening calculation for both the upper and lower segments of the McCallum Creek fault and the uncertainties associated with using thermochronometry to estimate total exhumation. However, the amount of shortening related to the foreland thrust system and out-of-sequence slip on the McCallum Creek fault are relatively well bracketed, and the  $^{40}$ Ar/ $^{39}$ Ar glass age of  $3.80 \pm 0.05$  Ma marking the maximum timing of onset for these events has nearly negligible uncertainty compared to our other age information. Late Pliocene and younger deposits

are used to calculate slip rates on the Denali fault and thrusts in the Northern Foothills fold and thrust belt (Matmon et al., 2006; Mériaux et al., 2009; Bemis et al., 2015; Haeussler, et al., 2017b). Therefore, calculating a shortening rate for the McCallum Creek thrust system since ca. 3.8 Ma rather than 6 Ma is more useful to compare with published rates on the Denali fault, Totschunda fault, and in the Northern Foothills fold and thrust belt. Our preferred shortening values for the foreland thrust system range from 557 m (cross section B) to 1017 m (cross section C) (Fig. 9). Exposure of the upper McCallum Creek fault crosscutting foreland folds yields at least 1350 m of out-of-sequence shortening on the main McCallum Creek fault after ca. 3.8 Ma. Combining these shortening estimates results in ~1900-2350 m of shortening since ca. 3.8 Ma and produces a shortening rate of 0.5–0.6 mm/yr oriented at ~005–185, approximately perpendicular to the Denali fault. The prospect that evidence for additional shortening has been eroded away and absent constraints on when exactly the foreland thrust system initiated after 3.8 Ma make this shortening rate estimate a minimum. The low-dip Granite Mountain fault north of the Denali fault and east of the Delta River (Fig. 2) has a documented late Pliocene-Present shortening rate of 1-4 mm/yr perpendicular to the Denali fault (Bemis et al., 2015). Documenting post-3.8 Ma shortening in the McCallum Creek thrust system thus increases the known geologically determined convergence rate in this section of the Denali fault system by up to ~60% and complements other geological data sets used to decipher regional active deformation in southern Alaska (e.g., Bemis et al., 2012).

#### Strike-Slip Translation and Continued Shortening

The current data record ~7 m.y. of shortening on the McCallum Creek thrust system while it was being translated to the northwest by dextral slip on the Denali fault. Our combined structural and thermochronological data set complements stratigraphic information from the McCallum Formation, which suggests the Totschunda fault played a role in the late Miocene reactivation of the McCallum Creek fault and related foreland basin evolution. Bemis et al. (2015) show that the geometry of the Denali-Totschunda fault-fault triple junction requires convergence. They call on this convergence as a mechanism to explain thrust faulting north of the Denali fault, which appears to have primarily developed after the mid-Pliocene (Bemis and Wallace, 2007). We expand upon their model and propose that communication between the Denali and Totschunda faults at ca. 7 Ma caused the region southwest of the triple junction (modern McCallum Creek area) to experience convergence (Fig. 13). The convergence may have resulted in flexural upwarping and distributed slip on new and preexisting structures near the triple junction. In our model, the region of upwarping and distributed faulting would initiate rapid cooling and evolve over time into slip along the throughgoing McCallum Creek fault. A region of flexural subsidence adjacent to the structural upwarping would provide accommodation space for the McCallum Formation and is corroborated by the presence of a low, swampy environment southwest of the Denali-Totschunda intersection today (Fig. 13). The abrupt facies transition in the McCallum Formation (Fig. 5) probably records the switch from distributed faulting to localized thrust slip on the main McCallum Creek fault. Due to paired dextral slip on the Denali and Totschunda faults, the McCallum Creek fault, the McCallum foreland basin, and Denali-Totschunda intersection all have been migrating to the northwest along the Denali fault (Bemis et al., 2015) (Fig. 13). Because both the Totschunda fault and Denali fault east of the triple junction feed slip onto the Denali fault west of the triple junction, the McCallum Creek thrust system and foreland basin are being translated at a faster rate than the triple junction.

Deformed Miocene-Pliocene strata (Nokleberg et al., 2015) and ca. 2 Ma AHe cooling ages (Fitzgerald et al., 2017) suggest that shortening has been occurring on the Slate Creek fault system between the College glacier and Denali-Totschunda intersection throughout the Pliocene and Quaternary. Shortening along the Slate Creek fault system is likely the along-strike continuation of shortening here documented for the McCallum Creek thrust system. Therefore, we amend the tectonic model of Bemis et al. (2015), which suggests that convergence from the Denali-Totschunda triple junction is primarily absorbed by thrust faults north of the Denali fault. As an addendum to their model, we propose that dextral strike-slip faulting on the Totschunda fault has been ongoing since at least 7 Ma and likely earlier (ca. 25 Ma; Milde, 2014). We infer that shortening introduced by the inherently unstable Denali-Totschunda triple junction was accommodated by the McCallum Creek fault south of the Denali fault from the late Miocene until the mid-Pliocene. At ca. 3 Ma, convergence from the triple junction was transferred to north of the Denali fault and is recorded by rapid growth and regional advance of the Northern Foothills fold and thrust belt (Bemis and Wallace, 2007; Benowitz et al., 2015) (Fig. 13). Interestingly, advance of the Northern Foothills fold and thrust belt is broadly contemporaneous with development of the McCallum foreland thrust system. Assuming regional block motion is constant over the past ~7 m.y., the rapid late Pliocene-Quaternary shortening north of the Denali fault would predict a reduction in the shortening rate on structures to the south. The folded Pliocene strata, tilted Quaternary glacial strata, potentially warped Quaternary surfaces, incised stream segments, and historic seismicity provide evidence for Quaternary deformation in the McCallum Creek thrust system, albeit at a potentially lower rate than during the late Miocene and Pliocene.

# Role of the McCallum Creek Fault in Southern Alaska Tectonics

## Regional Plate Motion

Southern Alaska has been argued to deform as a series of rigid blocks (Lahr and Plafker, 1980) or as a continuum (Finzel et al., 2011a). Aside from these opposing rheologic models, lithospheric motion in southern Alaska has been interpreted to reflect block rotation (Stout and Chase, 1980), a collisional indenter (Mériaux et al., 2009), or lateral extrusion (Redfield et al., 2007). Haeussler et al. (2017b) provides a synopsis of these various tectonic scenarios.

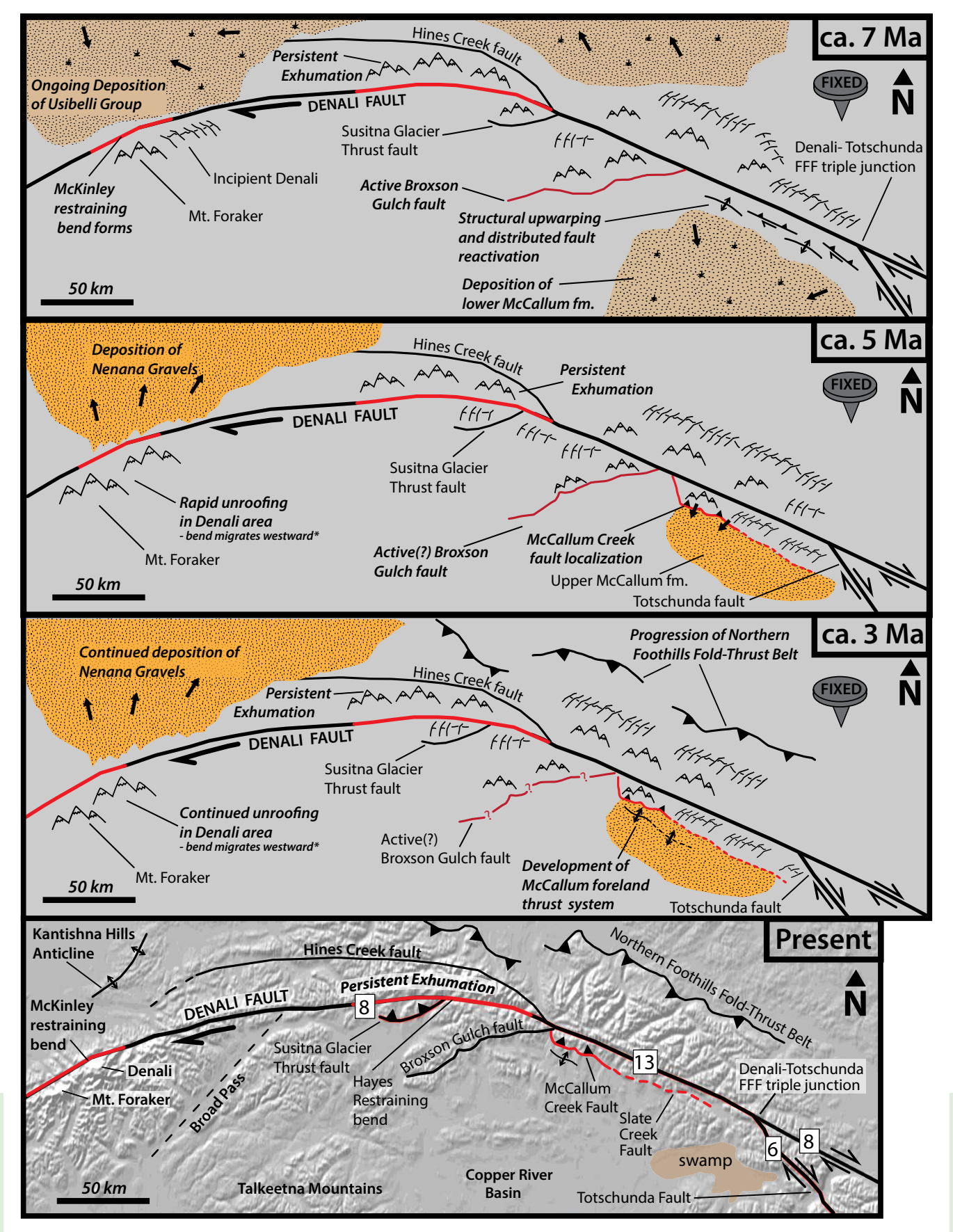


Figure 13. Tectonic model showing the evolution of the McCallum Creek thrust system and other components of the Denali fault system since ca. 7 Ma. Locations of features south of the Denali fault are restored using the geologic slip rates from Haeussler et al. (2017b), which are shown on the "Present" frame (in mm/yr). Arrows are fluvial flow indicators generalized from Ridgway et al. (2007), Brennan and Ridgway (2015), and Allen (2016). Fault sections illuminated in red are hypothesized to drive local rock exhumation based on work by Fitzgerald et al. (1993, 1995), Benowitz et al. (2011, 2014), Perry (2014), Waldien et al. (2017), and this study. \*Migration of the McKinley restraining bend is based on the work of Burkett et al. (2016) and Bemis et al. (2015). Image inspired by Riccio et al. (2014).

**Research Paper** 

Our analysis of the McCallum Creek thrust system increases the known geologically determined convergence rate across the Denali fault system in the eastern Alaska Range by 0.5–0.6 mm/yr. Even with the increased convergence rate, the total Denali fault-normal shortening rate is not sufficient to justify the collisional indenter mode of deformation in southern Alaska (e.g., Mériaux et al., 2009). Haeussler et al. (2017b) propose a model for southern Alaska tectonics involving a combination of the collisional indenter, block rotation, and lateral extrusion models. Our analysis of the McCallum Creek thrust system is compatible with the combined rotation, indentation, and extrusion model and supports rigid block motion as the primary style of deformation between the Aleutian subduction zone and the eastern Alaska Range.

As part of their integrated tectonic model, Haeussler et al. (2017b) propose that active thrust systems at the southern margin of the Alaska Range strike oblique to the Denali fault and have the effect of reducing the dextral slip rate. Rather, we have documented that the thrust section of the McCallum Creek fault strikes nearly parallel to the adjacent section of the Denali fault, and the shortening direction is approximately perpendicular to the Denali fault, thus causing it to accommodate primarily the collisional component of relative plate motion.

#### Geodynamic Considerations for Southern Alaska

Several lines of evidence suggest a widespread tectonic event occurred in southern Alaska in the late Miocene. The record of this tectonic event in the Alaska Range includes initiation of rapid exhumation of Denali (Fitzgerald et al., 1993, 1995), rapid cooling in the western Alaska Range (Haeussler et al., 2008), rapid deposition of a thick sequence of coarse clastic strata on the north flank of the eastern Alaska Range (Ridgway et al., 2007; Trop and Ridgway, 2007), and development of a rain shadow across the range (Bill et al., 2018). The Wrangell volcanic field also displays an increase in magmatism at this time (Preece and Hart, 2004; Benowitz and Addison, 2017) (Fig. 2). Late Miocene thrusting and related hanging wall exhumation in the McCallum Creek area are coeval with these events and provide additional evidence for a fundamental change in the Denali fault system in the late Miocene. Fitzgerald et al. (1993, 1995) attribute onset of rapid cooling in the Denali area at this time to a change in PAC-NA relative plate motion. Clockwise rotation of the Pacific plate vector relative to the southern Alaska margin by 5°-15° sometime ca. 8-6 Ma (Atwater and Stock, 1998; Doubrovine and Tarduno, 2008; Austermann et al., 2011) is a mechanism to increase convergence along the Denali fault system at this time (Jadamec et al., 2013). The late Miocene may also correspond to the onset of instability at the PAC-NAM-YAK triple junction and southward propagation of the YAK-NAM convergent margin (Enkelmann et al., 2008; Gulick et al., 2013). The difficulties in direct dating of fault slip and orogenic growth preclude a causal relationship between a plate motion vector change and orogenic events in the Alaska Range. However, the time progression of tectonic adjustments, exhumation, and basin evolution suggests that these plate margin processes are linked (Finzel et al., 2011b). Thus, rapid exhumation, basin evolution, and growth of the Alaska Range in the late Miocene likely represent a far-field response to plate margin adjustments at the southern Alaska plate margin. Evidence of plate margin processes recorded in the Alaska Range requires that a significant portion of the crust between the southern Alaska plate margin and the Denali fault is moving as a rigid block in order to transfer PAC-NAM-YAK convergence not accommodated near the plate margin to thrust faults in the Alaska Range.

# Implications for Splay Thrust Faults in Continental Strike-Slip Fault Systems

The role of thrust faults within continental strike-slip fault systems has long been recognized, and the seismic risk associated with them has generated significant interest. Much of what is known about the development of these splay thrust systems is the result of historic seismicity in the San Andreas fault system (e.g., Namson and Davis, 1988). Thrust systems linked to the Denali fault display both similarities and differences when compared to those in the San Andreas fault system. Because the McCallum Creek thrust system is a well exposed, young, and actively evolving thrust system, it may provide further insight to the mechanics of thrust systems splaying from continental strike-slip faults.

On the basis of our structural and cooling age data, it appears that splay thrust systems may initiate as a suite of distributed faults. As the thrust system matures, some faults may become abandoned as slip is localized on a single throughgoing thrust (or reverse) fault. In our field area, we observe that the Mc-Callum Creek fault has been the key reverse fault since the late Miocene, but the Hoodoo fault and unnamed fault at the southern margin of the plutonic complex also have experienced mid-late Cenozoic slip. Although these faults offset Eocene volcanic strata in the hanging wall of the McCallum Creek fault, most AFT cooling ages are uniform across them. It is possible that the Hoodoo fault and the unnamed fault bounding the plutonic complex were active as strike-slip and/or reverse faults during the Miocene and became less active by the time that most hanging wall rocks passed through the AFT partial annealing zone at ca. 6 Ma. Alternatively, the faults may not have had enough vertical slip to offset the ca. 6 Ma AFT ages. Both the stratigraphy of the McCallum foreland and hanging wall cooling ages suggest that the McCallum Creek fault was the primary contractional structure by ca. 5 Ma. Thus, our estimates of the timing of fault slip in the field area appear to record a transition from early distributed reverse and dextral faulting to localized slip on a throughgoing reverse fault (Fig. 12).

Once convergence initiates and a throughgoing thrust (or reverse) fault is established, the shortening direction may be constant throughout the various phases of thrust system evolution and as it is translated along the strike-slip margin. We observe that the McCallum Creek thrust system has accommodated shortening in the same direction for ~7 m.y. while being translated along a nearly straight section of the Denali fault. During this continued shortening, rocks in the hanging wall of the McCallum Creek fault were exhumed from below the AFT partial annealing zone to the surface. These findings contrast

strongly with observations of shortening structures found in restraining steps and bends, which typically facilitate rapid shortening and uplift rates but are generally too short-lived to accumulate significant finite shortening or exhumation (Wesnousky, 1988; Wakabayashi et al., 2004; Roeske et al., 2007). Thus, we propose that long-lived splay thrust systems provide a mechanism for accommodating the convergent component of wholesale oblique plate motion and are thus recorders of long-term plate motion, rather than short-lived structural complexities. The combined structural-stratigraphic information contained in the McCallum Creek field area also documents that active thrust fault systems are a primary mode of generating elevated topography in strike-slip dominated orogens.

Background seismicity in the Denali and San Andreas fault systems yields contradictory records of the seismic hazard posed by splay thrust systems. Seismicity in the California Coast Ranges records active deformation on both strike-slip and thrust faults within the San Andreas fault system (Seeber and Armbruster, 1995). Alternatively, stress inversions of background seismicity in the Alaska Range prior to the 2002 M<sub>w</sub> 7.9 Denali earthquake primarily reflect dextral faulting with minimal convergence (Ratchkovski et al., 2004). In contrast to the pre-2002 background seismicity, aftershock clusters from the Denali earthquake record significant shortening across the Denali fault (Vallage et al., 2014). This transition is also recorded by the rotation of stress axes in the stress-tensor inversions (Ratchkovski et al., 2004) (Fig. 8). Together, these records of historic seismicity in the Alaska Range suggest that thrust faults in the area do not produce significant background seismicity and instead fail during large strike-slip earthquakes due to coseismic linkage with the strike-slip fault. This kinematic linkage was directly observed in 2002, when the M., 7.9 Denali event initiated on the Susitna Glacier thrust fault and propagated onto the Denali fault. Seismicity was also recorded on the McCallum Creek fault during the 2002 event (Brocher et al., 2004; Ratchkovski et al., 2004) (Fig. 4).

Both similarities and differences exist between splay thrust systems and regional fold and thrust belts. In our analysis of the McCallum Creek thrust system, we observe that: (1) material is eroded from the hanging wall of the master reverse fault and deposited onto the footwall; (2) the thrust system propagated and shifted the deformation front into the foreland basin; (3) out-of-sequence slip on a hinterland structure postdated development of the foreland thrusts; and (4) the resulting cross-sectional shape of the thrust system and foreland basin mimics that of a critical taper wedge. Subsets of these features have been documented in thrust systems connected to strike-slip faults in the California Coast Ranges (Namson et al., 1990; Unruh and Moores, 1992; Unruh et al., 1992), Anatolia (Lyberis et al., 1992), the Southern Alps (Norris and Cooper, 1997), and the Indo-Asia collision zone (Allen et al., 1999; Yin et al., 2002, 2008; Selander et al., 2012). Although the features of fault slip are similar between thrust systems bounding transpressional orogens and regional fold and thrust belts, the master shortening structures in transpressional orogens may initiate and persist as moderate or steeply dipping faults (e.g., Davis et al., 2005; Gold et al., 2006; Selander et al., 2012; this study). As a result, the developing orogenic wedge in a transpressional orogen may display a steeper taper angle

than those commonly observed in classic fold and thrust belts (e.g., Jamieson and Beaumont, 2013). There are a number of reasons why thrust systems splaying from continental strike-slip faults would behave differently than fold and thrust belts. These include: (1) interference between the regional stresses related to the strike-slip fault system and stresses in the wedge; (2) kinematic linkage between the strike-slip fault and the thrust system; (3) inherited faults controlling where shortening structures develop; (4) the lack of detachment horizons in regionally continuous sedimentary strata (i.e., platform sediments); and (5) changes in the mechanical stratigraphy of the crust across the strike-slip fault. Here, we recognize the commonalities between thrust systems in transpressional orogens and regional fold and thrust belts, but we propose that the two modes of crustal deformation are not entirely equivalent.

#### CONCLUSIONS

The McCallum Creek thrust system has accommodated active convergence as part of the Denali fault system since at least the late Miocene and continues to be active in the present. Reverse faulting on the main McCallum Creek fault and thrusting on an imbricate system of blind thrusts in the foreland have accommodated ~5.5 km of shortening and ~4 km of bedrock exhumation since hanging wall rocks passed through AFT closure at ca. 6 Ma. Shortening on the McCallum Creek thrust system is, and has been, synchronous with dextral slip on the Denali fault, thereby creating a set of interconnected structures that absorb oblique plate motion. Our middle Pliocene-Present shortening rate estimate of 0.5-0.6 mm/yr for the McCallum Creek thrust system increases the known active shortening across the eastern Alaska Range by up to ~60% and demonstrates that significant shortening in the Denali fault system has been occurring east of the curved section of the Denali fault since at least 6 Ma. Late Miocene convergence, basin development, and rapid cooling in the Mc-Callum Creek area may have developed due to coeval slip on the Denali and Totschunda faults. Continued basin development and exhumation in the Mc-Callum Creek area record Pliocene-Quaternary slip on the McCallum Creek fault and outward growth of the Alaska Range orogen. Development of the McCallum Creek thrust system, as a component of the actively evolving Denali fault system, is a far-field response to Neogene modification of the southern Alaska plate boundary.

#### **ACKNOWLEDGMENTS**

We thank Patrick Terhune, Kailyn Davis, Bob Gillis, and Paul Layer for field assistance. Eric Cowgill provided valuable and thorough feedback on an early version of this manuscript. This research was funded by the University of California–Davis Durrell graduate student research fund, American Association of Petroleum Geologists, Alaska Geological Society, and Geological Society of America grants to Waldien; National Science Foundation (NSF) grants 1450730, 1249885, and 1434656 to Benowitz; NSF grant 0952834 to Roeske; and NSF grant 1550034 to Ridgway. Figures 7, 9, and all geologic cross sections were made using Rick Allmendinger's Stereonet, FaultKin, and AreaErrorProp programs. We thank reviewers Rich Koehler and Adam Forte and guest associate editor James Jones for insightful and constructive comments on the manuscript.

#### REFERENCES CITED

- Ager, T.A., 2007, Vegetation response to climate change in Alaska: Examples from the fossil record: U.S. Geological Survey Open-File Report 2007-1096, 47 p.
- Allen, M.B., Vincent, S.J., and Wheeler, P.J., 1999, Late Cenozoic tectonics of the Kepingtage thrust zone: Interactions of the Tien Shan and Tarim Basin, northwest China: Tectonics, v. 18, no. 4, p. 639–654, https://doi.org/10.1029/1999TC900019.
- Allen, W.K., 2016, Miocene-Pliocene strike-slip basin development along the Denali fault system in the eastern Alaska Range: Chronostratigraphy and provenance of the McCallum Formation and implications for displacement [M.S. thesis]: West Lafayette, Indiana, Purdue University. 160 o.
- Allen, W.K., Ridgway, K.D., Benowitz, J.A., Waldien, T.S., and Roeske, S.M., 2014, Neogene Transpressional Basin Development along the Denali Fault System in the Eastern Alaska Range: The Stratigraphy of the McCallum Basin and Implications for Displacement along the Denali Fault System: Geological Society of America Abstracts with Programs, v. 46, no. 6, p. 364.
- Allmendinger, R.W., Cardozo, N., and Fisher, D., 2012, Structural Geology Algorithms: Vectors and Tensors in Structural Geology: New York, Cambridge University Press, 304 p.
- Atwater, T., and Stock, J., 1998, Pacific–North America Plate Tectonics of the Neogene South-western United States: An Update: International Geology Review, v. 40, p. 375–402, https://doi.org/10.1080/00206819809465216.
- Austermann, J., Ben-Avraham, Z., Bird, P., Heidbach, O., Schubert, G., and Stock, J.M., 2011, Quantifying the forces needed for the rapid change of Pacific plate motion at 6 Ma: Earth and Planetary Science Letters, v. 307, no. 3, p. 289–297, https://doi.org/10.1016/j.epsl.2011 .04.043.
- Batir, J.F., Blackwell, D.D., and Richards, M.C., 2013, Updated Heat Flow of Alaska: Alaska Energy Authority/Alaska Center for Energy and Power, 47 p.
- Bemis, S.P., and Wallace, W.K., 2007, Neotectonic framework of the north-central Alaska Range foothills, in Ridgway, K.D., Trop, J.M., Glen, J.M.G., and O'Neill, M.O., eds., Tectonic Growth of a Collisional Continental Margin: Crustal Evolution of Southern Alaska: Geological Society of America Special Paper 431, p. 549–572, https://doi.org/10.1130/2007.2431(21).
- Bemis, S.P., Carver, G.A., and Koehler, R.D., 2012, The Quaternary thrust system of the northern Alaska Range: Geosphere, v. 8, no. 1, p. 196–205, https://doi.org/10.1130/GES00695.1.
- Bemis, S.P., Weldon, R.J., and Carver, G.A., 2015, Slip partitioning along a continuously curved fault: Quaternary geologic controls on Denali fault system slip partitioning, growth of the Alaska Range, and the tectonics of south-central Alaska: Lithosphere, v. 7, no. 3, p. 235–246, https://doi.org/10.1130/L352.1.
- Benowitz, J., and Addison, J., 2017, Developing a Tephra Database for IODP sites U1417 and U1418: Late Miocene to Present Evolution of Eruptive Volcanism along the Gulf of Alaska: Geological Society of America Abstracts with Programs, v. 49, no. 4, https://doi.org/10.1130 /abs/2017CD-29892.
- Benowitz, J.A., Fowell, S.J., Addison, J., and Layer, P., 2007, Tectonic and paleoclimatic significance of Early Pliocene palynofloras from the southwestern Alaska Range: Geological Society of America Abstracts with Programs, v. 39, no. 4, p. 53.
- Benowitz, J.A., Layer, P.W., Armstrong, P., Perry, S.E., Haeussler, P.J., Fitzgerald, P.G., and Vanlaningham, S., 2011, Spatial variations in focused exhumation along a continental-scale strikeslip fault: The Denali fault of the eastern Alaska range: Geosphere, v. 7, no. 2, p. 455–467, https://doi.org/10.1130/GES00589.1.
- Benowitz, J.A., Haeussler, P.J., Layer, P.W., O'Sullivan, P.B., Wallace, W.K., and Gillis, R.J., 2012, Cenozoic tectono-thermal history of the Tordrillo Mountains, Alaska: Paleocene–Eocene ridge subduction, decreasing relief, and late Neogene faulting: Geochemistry, Geophysics, Geosystems, v. 13, p. 1–22, https://doi.org/10.1029/2011GC003951.
- Benowitz, J.A., Layer, P.W., and Vanlaningham, S., 2014, Persistent long-term (c. 24 Ma) exhumation In the Eastern Alaska Range constrained by stacked thermochronology, *in Jourdan*, F, et al., eds., Advances in 40Ar/39Ar Dating: From Archaeology to Planetary Sciences: Geological Society of London Special Publications, v. 378, no. 1, p. 225–243, https://doi.org/10.1144/SP378.12.
- Benowitz, J.A., Gilles, R.J., O'Sullivan, P.B., Fitzgerald, P.G., Bemis, S.P., Roeske, S.M., Terhune, P., Nokleberg, W.J., 2015, A Thermochronological Perspective on the Cenozoic Tectonics Along the Denali Fault System Across Alaska: Geological Society of America Abstracts with Programs, v. 47, no. 4, p. 61.
- Benowitz, J.A., Layer, P.W., Wypych, A., and Twelker, E., 2017, 40Ar/39Ar data from rocks collected in the 2015 Wrangellia mineral assessment project area, Mount Hayes A-5, Mount Hayes

- B-6, and Talkeetna Mountains D-2 quadrangles, Alaska: Alaska Division of Geological & Geophysical Surveys raw Data File 2017-1, p. 9, https://doi.org/10.14509/29699.
- Betka, P.M., Gillis, R.J., and Benowitz, J.A., 2017, Cenozoic sinistral transpression and polyphase slip within the Bruin Bay fault system, Iniskin-Tuxedni region, Cook Inlet, Alaska: Geosphere, v. 13, p. 1806–1833, https://doi.org/10.1130/GES01464.1.
- Bill, N.S., Mix, H.T., Clark, P.U., Reilly, S.P., Jensen, B.J., and Benowitz, J.A., 2018, A stable isotope record of late Cenozoic surface uplift of southern Alaska: Earth and Planetary Science Letters, v. 482, p. 300–311, https://doi.org/10.1016/j.epsl.2017.11.029.
- Brennan, P.R.K., and Ridgway, K.D., 2015, Detrital zircon record of Neogene exhumation of the central Alaska Range: A far-field upper plate response to flat-slab subduction: Geological Society of America Bulletin, v. 127, p. 945–961, https://doi.org/10.1130/B31164.1.
- Brennan, P.R.K., Gilbert, H., and Ridgway, K.D., 2011, Crustal structure across the central Alaska Range: Anatomy of a Mesozoic collisional zone: Geochemistry, Geophysics, Geosystems, v. 12, no. 4, Q04010, https://doi.org/10.1029/2011GC003519.
- Bond, G.C., 1973, A late Paleozoic volcanic arc in the eastern Alaska Range, Alaska: The Journal of Geology, v. 81, p. 557–575, https://doi.org/10.1086/627907.
- Bond, G.C., 1976, Geology of the Rainbow Mountain-Gulkana Glacier Area, Eastern Alaska Range, with Emphasis on Upper Paleozoic Strata: State of Alaska Geologic Division of Geological & Geophysical Surveys Geologic Report 45, 47 p., scale 1:40:000, 3 sheets.
- Brocher, T.M., Fuis, G.S., Lutter, W.J., Christensen, N.I., and Ratchkovski, N.A., 2004, Seismic velocity models for the Denali fault zone along the Richardson Highway, Alaska: Bulletin of the Seismological Society of America, v. 94, p. 85–106, https://doi.org/10.1785/0120040615.
- Burkett, C.A., Bemis, S.P., and Benowitz, J.A., 2016, Along-fault migration of the Mount McKinley restraining bend of the Denali fault defined by late Quaternary fault patterns and seismicity, Denali National Park & Preserve, Alaska: Tectonophysics, v. 693, p. 489–506, https://doi.org /10.1016/j.tecto.2016.05.009.
- Colpron, M., and Nelson, J.L., 2011, A Digital Atlas of Terranes for the Northern Cordillera: British Columbia Ministry of Energy and Mines, BCGS GeoFile 2011-11.
- Crone, A.J., Personius, S.F., Craw, P.A., Haeussler, P.J., and Staft, L.A., 2004, The Susitna glacier thrust fault: Characteristics of surface ruptures on the fault that initiated the 2002 Denali fault earthquake: Bulletin of the Seismological Society of America, v. 94, p. 5–22, https://doi .org/10.1785/0120040619.
- Davis, K., Burbank, D.W., Fisher, D., Wallace, S., and Nobes, D., 2005, Thrust-fault growth and segment linkage in the active Ostler fault zone, New Zealand: Journal of Structural Geology, v. 27, no. 8, p. 1528–1546, https://doi.org/10.1016/j.jsg.2005.04.011.
- Doblas, M., 1998, Slickenside kinematic indicators: Tectonophysics, v. 295, p. 187–197, https://doi.org/10.1016/S0040-1951(98)00120-6.
- Donelick, R.A., Ketcham, R.A., and Carlson, W.D., 1999, Variability of apatite fission-track annealing kinetics: II. Crystallographic orientation effects: The American Mineralogist, v. 84, p. 1224–1234, https://doi.org/10.2138/am-1999-0902.
- Donelick, R.A., O'Sullivan, P.B., and Ketcham, R.A., 2005, Apatite Fission-Track Analysis: Reviews in Mineralogy and Geochemistry, v. 58, p. 49–94, https://doi.org/10.2138/rmg.2005.58.3.
- Doser, D.I., 2004, Seismicity of the Denali-Totschunda fault zone in central Alaska (1912–1988) and its relation to the 2002 Denali fault earthquake sequence: Bulletin of the Seismological Society of America, v. 94, p. 132–144, https://doi.org/10.1785/0120040611.
- Doubrovine, P.V., and Tarduno, J.A., 2008, A revised kinematic model for the relative motion between Pacific oceanic plates and North America since the Late Cretaceous: Journal of Geophysical Research. Solid Earth, v. 113, p. 1–20, https://doi.org/10.1029/2008JB005585.
- Dusel-Bacon, C., Holm-Denoma, C.S., Jones, J.V., Aleinikoff, J.N., and Mortensen, J.K., 2017, Detrital zircon geochronology of quartzose metasedimentary rocks from parautochthonous North America, east-central Alaska: Lithosphere, v. 9, no. 6, p. 927–952, https://doi.org/10. 1130/L672.1.
- Eberhart-Phillips, D., Haeussler, P.J., Freymueller, J.T., Frankel, A.D., Rubin, C.M., Craw, P., Ratch-kovski, N.A., Anderson, G., Carver, G.A., Crone, A.J., Dawson, T.E., Fletcher, H., Hansen, R., Harp, E.L., et al., 2003, The 2002 Denali fault earthquake, Alaska: A large magnitude, slip-partitioned event: Science, v. 300, p. 1113–1118, https://doi.org/10.1126/science.1082703.
- Eberhart-Phillips, D., Christensen, D.H., Brocher, T.M., Hansen, R., Ruppert, N.A., Haeussler, P.J., and Abers, G.A., 2006, Imaging the transition from Aleutian subduction to Yakutat collision in central Alaska, with local earthquakes and active source data: Journal of Geophysical Research, v. 111, B11303, https://doi.org/10.1029/2005JB004240.

- Elliott, J., Freymueller, J.T., and Larsen, C.F., 2013, Active tectonics of the St. Elias orogen, Alaska, observed with GPS measurements: Journal of Geophysical Research. Solid Earth, v. 118, p. 5625–5642, https://doi.org/10.1002/jgrb.50341.
- Enkelmann, E., Garver, J.I., and Pavlis, T.L., 2008, Rapid exhumation of ice-covered rocks of the Chugach–St. Elias orogen, Southeast Alaska: Geology, v. 36, p. 915–918, https://doi.org/10 .1130/G2252A.1.
- Eppelbaum, L., Kutasov, I., and Pilchin, A., 2014, Applied Geothermics: Heidelberg-New York-Dordrecht-London, Springer, 267 p., https://doi.org/10.1007/978-3-642-34023-9.
- Erdman, C.F., and Kelsey, H.M., 1992, Pliocene and Pleistocene stratigraphy and tectonics, Ohara Depression and Wakarara Range, North Island, New Zealand: New Zealand Journal of Geology and Geophysics, v. 35, p. 177–192, https://doi.org/10.1080/00288306.1992.9514512.
- Finzel, E.S., Flesch, L.M., and Ridgway, K.D., 2011a, Kinematics of a diffuse North America– Pacific–Bering plate boundary in Alaska and western Canada: Geology, v. 39, no. 9, p. 835– 838, https://doi.org/10.1130/G32271.1.
- Finzel, E.S., Trop, J.M., Ridgway, K.D., and Enkelmann, E., 2011b, Upper plate proxies for flatslab subduction processes in southern Alaska: Earth and Planetary Science Letters, v. 303, p. 348–360, https://doi.org/10.1016/j.epsl.2011.01.014.
- Fisher, M.A., Ratchkovski, N.A., Nokleberg, W.J., Pellerin, L., and Glen, J.M.G., 2004, Geophysical Data Reveal the Crustal Structure of the Alaska Range Orogen within the Aftershock Zone of the Mw 7.9 Denali Fault Earthquake: Bulletin of the Seismological Society of America, v. 94, no. 6B, p. S107-S131, https://doi.org/10.1785/0120040613.
- Fitzgerald, P.G., Stump, E., and Redfield, T.E., 1993, Late Cenozoic uplift of Denali and its relation to relative plate motion and fault morphology: Science, v. 259, p. 497–499, https://doi.org/10.1126/science.259.5094.497.
- Fitzgerald, P.G., Sorkhabi, R.B., Redfield, T.F., and Stump, E., 1995, Uplift and denudation of the central Alaska Range: A case study in the use of apatite fission track thermochronology to determine absolute uplift parameters: Journal of Geophysical Research, v. 100, p. 20,175– 20,191, https://doi.org/10.1029/95JB02150.
- Fitzgerald, P.G., Roeske, S.M., Benowitz, J.A., Riccio, S.J., Perry, S.E., and Armstrong, P.A., 2014, Alternating asymmetric topography of the Alaska range along the strike-slip Denali fault: Strain partitioning and lithospheric control across a terrane suture zone: Tectonics, v. 33, no. 8, p. 1519–1533, https://doi.org/10.1002/2013TC003432.
- Fitzgerald, P.G., Benowitz, J.A., Ridgway, K.D., Warfel, T.S., and Allen, W.K., 2017, The role of terrane rheology vs. fault geometry for mountain formation and exhumation along the Denali fault of south-central Alaska: Geological Society of America Abstracts with Programs, v. 49, no. 6, https://doi.org/10.1130/abs/2017AM-305797.
- Fletcher, H.J., and Freymueller, J.T., 2003, New constraints on the motion of the Fairweather fault, Alaska, from GPS observations: Geophysical Research Letters, v. 30, no. 3, https://doi.org/10.1029/2002GL016476.
- Fleuty, M., 1964, The description of folds: Proceedings of the Geologists' Association, v. 75, no. 4, p. 461–492.
- Gallagher, K., Brown, R.W., and Johnson, C., 1998, Fission track analysis and its application to geological problems: Annual Review of Earth and Planetary Sciences, v. 26, p. 519–572, https://doi.org/10.1146/annurev.earth.26.1.519.
- Gold, R.D., Cowgill, E.S., Wang, X.F., and Chen, X.H., 2006, Application of trishear fault-propagation folding to active reverse faults: Examples from the Dalong fault, Gansu Province, NW China: Journal of Structural Geology, v. 28, p. 200–219, https://doi.org/10.1016/j.jsg.2005.10 006
- Green, P.F., Duddy, I.R., Gleadow, A.J.W., Tingate, P.R., and Laslett, G.M., 1986, Thermal annealing of fission tracks in apatite: 1. A qualitative description: Chemical Geology, Isotope Geoscience Section, v. 59, p. 237–253, https://doi.org/10.1016/0168-9622(86)90074-6.
- Gulick, S.P.S., Reece, R.S., Christeson, G.L., Van Avendonk, H., Worthington, L.L., and Pavlis, T.L., 2013, Seismic images of the Transition fault and the unstable Yakutat-Pacific-North American triple junction: Geology, v. 41, no. 5, p. 571–574, https://doi.org/10.1130/G33900.1.
- Haeussler, P.J., 2008, An Overview of the Neotectonics of Interior Alaska: Far-Field Deformation from the Yakutat Microplate Collision, in Freymueller, J.T, Haeussler, P.J., Wesson, R.L., and Ekström, G., eds., Active Tectonics and Seismic Potential of Alaska: American Geophysical Union Monograph 179, p. 83–108, https://doi.org/10.1029/179GM05.
- Haeussler, P.J., Schwartz, D.P., Dawson, T.E., Stenner, H.D., Lienkaemper, J.J., Sherrod, B., Cinti, F.R., Montone, P., Craw, P.A., Crone, A.J., and Personius, S.F., 2004, Surface rupture and slip distribution of the Denali and Totschunda faults in the 3 November 2002 M 7.9 earthquake,

- Alaska: Bulletin of the Seismological Society of America, v. 94, p. 23–52, https://doi.org/10 1785/0120040626
- Haeussler, P.J., O'Sullivan, P., Berger, A.L., and Spotila, J.A., 2008, Neogene exhumation of the Tordrillo Mountains, Alaska, and correlations with Denali (Mount McKinley), in Freymueller, J.T, Haeussler, P.J., Wesson, R.L., and Ekström, G., eds., Active Tectonics and Seismic Potential of Alaska: American Geophysical Union Monograph 179, p. 269–285, https://doi.org/10 .1029/179GM15.
- Haeussler, P.J., Saltus, R.W., Stanley, R.G., Ruppert, N., Lewis, K., Karl, S.M., and Bender, A., 2017a, The Peters Hills basin, a Neogene wedge-top basin on the Broad Pass thrust fault, south-central Alaska: Geosphere, v. 13, p. 1464–1488, https://doi.org/10.1130/GES01487.1.
- Haeussler, P.J., Matmon, A., Schwartz, D.P., and Seitz, G.G., 2017b, Neotectonics of interior Alaska and the late Quaternary slip rate along the Denali fault system: Geosphere, v. 13, p. 1445–1463, https://doi.org/10.1130/GES01447.1.
- Hanson, L.G., 1963, Bedrock geology of the Rainbow Mountain area, Alaska Range, Alaska: Alaska Division of Mines and Minerals Geologic Report 2, 82 p., 2 sheets, scale 1:42,240.
- Harrison, T.M., Célérier, J., Aikman, A.B., Hermann, J., and Heizler, M.T., 2009, Diffusion of <sup>40</sup>Ar in muscovite: Geochimica et Cosmochimica Acta, v. 73, p. 1039–1051, https://doi.org/10.1016/j.gca.2008.09.038.
- Hasebe, N., Barbarand, J., Jarvis, K., Carter, A., and Hurford, A.J., 2004, Apatite fission-track chronometry using laser ablation ICP-MS: Chemical Geology, v. 207, p. 135–145, https://doi. org/10.1016/j.chemgeo.2004.01.007.
- Hooke, R.L., 1968, Steady-state relationships on arid-region alluvial fans in closed basins: American Journal of Science, v. 266, no. 8, p. 609–629, https://doi.org/10.2475/ais.266.8.609.
- Jadamec, M.A., Billen, M.I., and Roeske, S.M., 2013, Three-dimensional numerical models of flat slab subduction and the Denali fault driving deformation in south-central Alaska: Earth and Planetary Science Letters, v. 376, p. 29–42, https://doi.org/10.1016/j.epsl.2013.06.009.
- Jamieson, R.A., and Beaumont, C., 2013, On the origin of orogens: Bulletin of the Geological Society of America, v. 125, p. 1671–1702, https://doi.org/10.1130/B30855.1.
- Judge, P.A., and Allmendinger, R.W., 2011, Assessing uncertainties in balanced cross sections: Journal of Structural Geology, v. 33, p. 458–467, https://doi.org/10.1016/j.jsg.2011.01.006.
- Kamb, W.B., 1959, Ice petrofabric observations from Blue Glacier, Washington, in relation to theory and experiment: Journal of Geophysical Research, v. 64, no. 11, p. 1891–1909, https:// doi.org/10.1029/JZ064i011p01891.
- Ketcham, R.A., 2005, Forward and reverse modeling of low-temperature thermochronology data, in Reiners, P.W., and Ehlers, T.A., eds., Low-Temperature Thermochronology: Techniques, Interpretations and Applications: Reviews in Mineralogy and Geochemistry, v. 58, p. 275–314.
- Ketcham, R.A., Donelick, R.A., and Carlson, W.D., 1999, Variability of apatite fission-track annealing kinetics: Ill. Extrapolation to geological time scales: The American Mineralogist, v. 84, p. 1235–1255, https://doi.org/10.2138/am-1999-0903.
- Koehler, R.D., 2013, Quaternary Faults and Folds (QFF): Alaska Division of Geological and Geophysical Surveys Digital Data Series 3, http://maps.dggs.alaska.gov/qff/.
- Kunk, M.J., 1995, 40Ar/39Ar Age-spectrum Data for Hornblende, Plagioclase and Biotite from Tephras Collected at Dan Creek and McCallum Creek, Alaska and in the Klondike Placer District Near Dawson, Yukon Territory: U.S. Geological Survey Open-File Report 95-0217A, 52 p.
- Lahr, J.C., and Plafker, G., 1980, Holocene Pacific-North American plate interaction in southern Alaska: Implications for the Yakataga seismic gap: Geology, v. 8, p. 483–486, https://doi.org/10.1130/0091-7613(1980)8<483:HPAPII>2.0.CO;2.
- Little, T.A., Cox, S., Vry, J.K., and Batt, G., 2005, Variations in exhumation level and uplift rate along the oblique-slip Alpine fault, central Southern Alps, New Zealand: Bulletin of the Geological Society of America, v. 117, p. 707–723, https://doi.org/10.1130/B25500.1.
- Lovera, O.M., Grove, M., and Harrison, T.M., 2002, Systematic analysis of K-feldspar <sup>40</sup>Ar/<sup>39</sup>Ar step heating results II: Relevance of laboratory argon diffusion properties to nature: Geochimica et Cosmochimica Acta, v. 66, no. 7, p. 1237–1255, https://doi.org/10.1016/S0016-7037 (01)00846-8.
- Lyberis, N., Yurur, T., Chorowicz, J., Kasapoglu, E., and Gundogdu, N., 1992, The East Anatolian Fault: An oblique collisional belt: Tectonophysics, v. 204, no. 1–2, p. 1–15, https://doi.org/10 .1016/0040-1951(92)90265-8.
- Marrett, R.A., and Allmendinger, R.W., 1990, Kinematic analysis of fault-slip data: Journal of Structural Geology, v. 12, p. 973–986, https://doi.org/10.1016/0191-8141(90)90093-E.

- Matmon, A., Schwartz, D.P., Haeussler, P.J., Finkel, R., Lienkaemper, J.J., Stenner, H.D., and Dawson, T.E., 2006, Denali fault slip rates and Holocene-late Pleistocene kinematics of central Alaska: Geology, v. 34, p. 645–648, https://doi.org/10.1130/G22361.1.
- Meisling, K.E., and Weldon, R.J., 1989, Late Cenozoic tectonics of the northwestern San Bernardino Mountains, southern California: Geological Society of America Bulletin, v. 101, no. 1, p. 106–128, https://doi.org/10.1130/0016-7606(1989)101<0106:LCTOTN>2.3.CO;2.
- Mériaux, A.-S., Sieh, K., Finkel, R.C., Rubin, C.M., Taylor, M.H., Meltzner, A.J., and Ryerson, F.J., 2009, Kinematic behavior of southern Alaska constrained by westward decreasing postglacial slip rates on the Denali fault, Alaska: Journal of Geophysical Research, v. 114, p. 1–19, https://doi.org/10.1029/2007JB005053.
- Milde, E.R., 2014, Using Low-Temperature Thermochronology to Constrain the Role of the Totschunda Fault in Southeastern Alaskan Tectonics [M.S. thesis]: Syracuse, New York, Syracuse University, 127 p.
- Miller, M.S., O'Driscoll, L.J., Porritt, R.W., and Roeske, S.M., 2018, Multiscale crustal architecture of Alaska inferred from P receiver function: Lithosphere, v. 10, no. 2, p. 267–278, https://doi.org/10.1130/L701.1.
- Morin, R.L., and Glen, J.M.G., 2003, Principal facts for 408 gravity stations in the vicinity of the Talkeetna Mountains, south-central Alaska: U.S. Geological Survey Open-File Report 03-27, 21 p.
- Namson, J.S., and Davis, T.L., 1988, Seismically active fold and thrust belt in the San Joaquin Valley, central California: Geological Society of America Bulletin, v. 100, p. 257–273, https://doi.org/10.1130/0016-7606(1988)100<0257:SAFATB>2.3.CO;2.
- Namson, J.S., Davis, T.L., and Lagoe, M.B., 1990, Tectonic history and fold-thrust deformation style of seismically active structures near Coalinga, in Rymer, M.J., and Ellsworth, W.L., eds., The Coalinga, California, Earthquake of May 2, 1983: U.S. Geological Survey Professional Paper 1487, p. 79–96.
- Nokleberg, W.J., Albert, N.R., Bond, G.C., Herzon, P.L., Miyaoka, R.T., Nelson, W.H., Richter, D.H., Smith, T.E., Stout, J.H., and Yeend, W., 1982, Geologic map of the southern part of Mount Hayes Quadrangle, Alaska, U.S. Geological Survey Open-File Report 82-52, 26 p., 1 sheet, scale 1:250.000.
- Nokleberg, W.J., Aleinikoff, J.N., Lange, I.M., Silva, S.R., Miyaoka, R.T., Schwab, C.E., and Zehner, R.E., 1992a, Preliminary geologic map of the Mount Hayes quadrangle, eastern Alaska Range, Alaska. U.S. Geological Survey Open-File Report 92-594, 39 p., 1 sheet, scale 1:250,000.
- Nokleberg, W.J., Aleinikoff, J.N., Dutro, J.T., Jr. Lanphere, M.A. Silberling, N.J., Silva, S.R., Smith, T.E., and Turner, D.L., 1992b, Map, tables, and summary of fossil and isotopic age data, Mount Hayes quadrangle, eastern Alaska Range, Alaska: U.S. Geological Survey Miscellaneous Field Studies Map 1996-D, 43 p., 1 sheet, scale 1:250,000.
- Nokleberg, W.J., Aleinikoff, J.N., Bundtzen, T.K., and Hanshaw, M.N., 2013, Geologic strip map along the Hines Creek fault showing evidence for Cenozoic displacement in the western Mount Hayes and northeastern Healy quadrangles, eastern Alaska Range, Alaska: U.S. Geological Survey Scientific Investigations Map 3238, pamphlet 29 p., scale 1:63,360, http://pubs.usgs.gov/sim/3238/.
- Nokleberg, W.J., Aleinikoff, J.N., Bond, G.C., Ferrians, O.J., Jr., Herzon, P.L., Lange, I.M., Miyaoka, R.T., Richter, D.H., Schwab, C.E., Silva, S.R., Smith, T.E., and Zehner, R.E., 2015, Geologic maps of the eastern Alaska Range, Alaska (44 quadrangles, 1:63,360 scale), with descriptions and interpretations of map units: Alaska Division of Geological & Geophysical Surveys Report of Investigation 2015-6, 64 p., 45 sheets, scale 1:63,360, https://doi.org/10.14509/29444.
- Norris, R.J., and Cooper, A.F., 1997, Erosional control on the structural evolution of a transpressional thrust complex on the Alpine Fault, New Zealand: Journal of Structural Geology, v. 19, no. 10, p. 1323–1342, https://doi.org/10.1016/S0191-8141(97)00036-9.
- Perry, S.E., 2014, Thermotectonic evolution of the Alaska Range: Low-temperature thermochronologic constraints [Ph.D. thesis]: Syracuse, New York, Syracuse University, 844 p.
- Petit, J.P., 1987, Criteria for the sense of movement on fault surfaces in brittle rocks: Journal of Structural Geology, v. 9, p. 597–608, https://doi.org/10.1016/0191-8141(87)90145-3.
- Plafker, G., Gilpin, L.M., and Lahr, J.C., 1994, Neotectonic map of Alaska, in Plafker, G., and Berg, H.C., eds., The Geology of North America, v. G1, The Geology of Alaska: Geological Society of America, plate 12, scale 1:2,500,000 with 3 tables and text.
- Preece, S.J., and Hart, W.K., 2004, Geochemical variations in the <5 Ma Wrangell volcanic field, Alaska: Implications for the magmatic and tectonic development of a complex continental arc system: Tectonophysics, v. 392, no. 1–4, p. 165–191, https://doi.org/10.1016/j.tecto.2004.04.011.

- Ratchkovski, N.A., Hansen, R.A., Stachnik, J.C., Cox, T., Fox, O., Rao, L., Clark, E., Lafevers, M., Estes, S., and MacCormack, J.B., 2003, Aftershock sequence of the Mw 7.9 Denali fault, Alaska, earthquake of 3 November 2002 from regional seismic network data: Seismological Research Letters, v. 74, p. 743–752, https://doi.org/10.1785/gssrl.74.6.743.
- Ratchkovski, N.A., Wiemer, S., and Hansen, R.A., 2004, Seismotectonics of the central Denali fault, Alaska, and the 2002 Denali fault earthquake sequence: Bulletin of the Seismological Society of America, v. 94, p. S156–S174, https://doi.org/10.1785/0120040621.
- Redfield, T.F., Scholl, D.W., Fitzgerald, P.G., and Beck, M.E., Jr., 2007, Escape tectonics and the extrusion of Alaska: Past, present, and future: Geology, v. 35, no. 11, p. 1039–1042, https://doi.org/10.1130/G23799A.1.
- Riccio, S.J., Fitzgerald, P.G., Benowitz, J.A., and Roeske, S.M., 2014, The role of thrust faulting in the formation of the eastern Alaska Range: Thermochronological constraints from the Susitna Glacier Thrust Fault region of the intracontinental strike-slip Denali Fault system: Tectonics, v. 33, no. 11, p. 2195–2217, https://doi.org/10.1002/2014TC003646.
- Richter, D.H., 1976, Geologic map of the Nabesna quadrangle, Alaska: U.S. Geological Survey Miscellaneous Investigations Series, Map I-932, 1 sheet, scale 1:250,000.
- Richter, D.H., and Matson, J.A., 1971, Quaternary faulting in the eastern Alaska Range: Bulletin of the Geological Society of America, v. 82, p. 1529–1540, https://doi.org/10.1130/0016-7606 (1971)82[1529:QFITEA]2.0.CO;2.
- Ridgway, K.D., Trop, J.M., Nokleberg, W.J., Davidson, C.M., and Eastham, K.R., 2002, Mesozoic and Cenozoic tectonics of the eastern and central Alaska Range: Progressive basin development and deformation in a suture zone: Geological Society of America Bulletin, v. 114, p. 1480–1504, https://doi.org/10.1130/0016-7606(2002)114<1480:MACTOT>2.0 .CO:2.
- Ridgway, K.D., Thoms, E.E., Layer, P.W., Lesh, M.E., White, J.M., and Smith, S.V., 2007, Neogene transpressional foreland basin development on the north side of the central Alaska Range, Usibelli Group and Nenana Gravel, Tanana basin, *in* Ridgway, K.D., Trop, J.M., Glen, J.M.G., and O'Neill, M.O., eds., Tectonic Growth of a Collisional Continental Margin: Crustal Evolution of Southern Alaska: Geological Society of America Special Paper 431, p. 507–547, https://doi.org/10.1130/2007.2431(20).
- Roeske, S.M., Till, A.B., Foster, D.A., and Sample, J.C., 2007, Introduction, in Till, A.B., Roeske, S.M., Sample, J.C., and Foster, D.A., eds., Exhumation Associated with Continental Strike-Slip Fault Systems: Geological Society of America Special Paper 434, p. 7–9, https://doi.org/10.1130/978-0-8137-2434-8(2007)434[wiir]2.0.CO;2.
- Rosenthal, J., Betka, P., Nadin, E., Gillis, R., and Benowitz, J., 2017, Vein formation during progressive Paleogene faulting and folding within the lower Cook Inlet basin, Alaska: Geosphere, v. 14, no. 1, p. 23–49, https://doi.org/10.1130/GES01435.1.
- Sanderson, D.J., and Marchini, W.R.D., 1984, Transpression: Journal of Structural Geology, v. 6, p. 449–458, https://doi.org/10.1016/0191-8141(84)90058-0.
- Seeber, L., and Armbruster, J.G., 1995, The San Andreas fault system through the Transverse Ranges as illuminated by earthquakes: Journal of Geophysical Research. Solid Earth, v. 100, B5, p. 8285–8310, https://doi.org/10.1029/94JB02939.
- Selander, J., Oskin, M., Ormukov, C., and Abdrakhmatov, K., 2012, Inherited strike-slip faults as an origin for basement-cored uplifts: Example of the Kungey and Zailiskey ranges, northern Tian Shan: Tectonics, v. 31, p. 1–22, https://doi.org/10.1029/2011TC003002.
- Spotila, J.A., House, M.A., Niemi, N.A., Brady, R.C., Oskin, M.E., and Buscher, J.T., 2007, Patterns of bedrock uplift along the San Andreas fault and implications for mechanisms of transpression, in Till, A.B., Roeske, S.M., Sample, J.C., and Foster, D.A., eds., Exhumation Associated with Continental Strike-Slip Fault Systems: Geological Society of America Special Paper 434, p. 15–33, https://doi.org/10.1130/2007.2434(02).
- Stein, R.S., and Ekström, G., 1992, Seismicity and geometry of a 110-km-long blind thrust fault 2. Synthesis of the 1982–1985 California Earthquake Sequence: Journal of Geophysical Research, v. 97, p. 4865–4883, https://doi.org/10.1029/91JB02847.
- Stout, J.H., 1965, Bedrock Geology between Rainy Creek and the Denali fault, Eastern Alaska Range, Alaska [M.S. thesis]: Fairbanks, University of Alaska, 75 p.
- Stout, J.H., and Chase, C.G., 1980, Plate kinematics of the Denali fault system: Canadian Journal of Earth Sciences, v. 17, p. 1527–1537, https://doi.org/10.1139/e80-160.
- Terhune, P., Benowiz, J., Waldien, T.S., Allen, W.K., Davis, K.N., Ridgway, K.D., Roeske, S.M., Fitzgerald, P.G., Brueseke, M.E., and O'Sullivan, P.B., 2015, Geochronological framework for the Cenozoic history of the southern Alaska Range fold and thrust belt: Geological Society of America Abstracts with Programs, v. 47, no. 4, p. 60.

- Tikoff, B., and Peterson, K., 1998, Physical experiments of transpression folding: Journal of Structural Geology, v. 20, p. 661–672, https://doi.org/10.1016/S0191-8141(98)00004-2.
- Trop, J.M., and Ridgway, K.D., 2007, Mesozoic and Cenozoic tectonic growth of southern Alaska: A sedimentary basin perspective, in Ridgway, K.D., Trop, J.M., Glen, J.M.G., and O'Neill, M.O., eds., Tectonic Growth of a Collisional Continental Margin: Crustal Evolution of Southern Alaska: Geological Society of America Special Paper 431, p. 55–94, https://doi.org/10.1130/2007.2431(04).
- Trop, J.M., Ridgway, K.D., Manuszak, J.D., and Layer, P., 2002, Mesozoic sedimentary-basin development on the allochthonous Wrangellia composite terrane, Wrangell Mountains basin, Alaska: A long-term record of terrane migration and arc construction: Geological Society of America Bulletin, v. 114, p. 693–717, https://doi.org/10.1130/0016-7606(2002)114-0693:MSBDOT>2.0.CO;2.
- Trop, J.M., Ridgway, K.D., and Sweet, A.R., 2004, Stratigraphy, palynology, and provenance of the Colorado Creek basin, Alaska, USA: Oligocene transpressional tectonics along the central Denali fault system: Canadian Journal of Earth Sciences, v. 41, no. 4, p. 457–480, https:// doi.org/10.1139/e04-003.
- Trop, J.M., Benowitz, J.M., Cole, R.B., and O'Sullivan, P.B., 2014, The Alaska Range suture zone: Latest Cretaceous arc volcanism and Oligocene strike-slip basin development and coeval dike swarms: Geological Society of America Abstracts with Programs, v. 46, no. 6, p. 781.
- Turner, D.L., and Smith, T.E., 1974, Geochronology and Generalized Geology of the Central Alaska Range, Clearwater Mountains, and Northern Talkeetna Mountains, Alaska: Alaska Division of Geological & Geophysical Surveys Open-File Report 72, 13 p., 1 sheet, scale 1:250,000.
- Twiss, R.J., and Unruh, J.R., 1998, Analysis of fault slip inversions: Do they constrain stress or strain rate?: Journal of Geophysical Research. Solid Earth, v. 103, p. 12,205–12,222, https:// doi.org/10.1029/98JB00612.
- Unruh, J.R., and Moores, E.M., 1992, Quaternary blind thrusting in the southwestern Sacramento Valley, California: Tectonics, v. 11, p. 192–203, https://doi.org/10.1029/91TC02494.
- Unruh, J.R., Sowers, J., Noller, J., and Lettis, W., 1992, Tectonic wedging and late Cenozoic evolution of the eastern Diablo Range mountain front, northwestern San Joaquin Valley, California: Field Guide to the Tectonics of the Boundary between the California Coast Ranges and the Great Valley of California: American Association of Petroleum Geologists Pacific Section Meeting, p. 13–22.
- Unruh, J.R., Twiss, R.J., and Hauksson, E., 1996, Seismogenic deformation field in the Mojave block and implications for tectonics of the eastern California shear zone: Journal of Geophysical Research, v. 101, p. 8335–8361, https://doi.org/10.1029/95JB03040.
- Vallage, A., Devès, M.H., Klinger, Y., King, G.C.P., and Ruppert, N.A., 2014, Localized slip and distributed deformation in oblique settings: The example of the Denali fault system, Alaska: Geophysical Journal International, v. 197, p. 1284–1298, https://doi.org/10.1093/qji/ggu100.

- Wakabayashi, J., Hengesh, J.V., and Sawyer, T.L., 2004, Four-dimensional transform fault processes: Progressive evolution of step-overs and bends: Tectonophysics, v. 392, no. 1, p. 279–301, https://doi.org/10.1016/j.tecto.2004.04.013.
- Waldien, T.S., 2015, Evolution of a Range-Boundary Thrust in a Strike Slip Fault System: The Late Miocene–Recent Slip History of the McCallum Creek Fault, Eastern Alaska Range, Alaska [M.S. thesis]: Davis, University of California, 119 p.
- Waldien, T.S., Roeske, S.M., and Stockli, D.F., 2016, Structural and thermal evolution of the Maclaren metamorphic belt, eastern Alaska Range, Alaska: Geological Society of America Abstracts with Programs, v. 48, no. 7, https://doi.org/10.1130/abs/2016AM-284224.
- Waldien, T.S., Roeske, S.M., Benowitz, J.A., and Stockli, D.F., 2017, Cenozoic reactivation of Cretaceous terrane accretionary structures in the eastern Alaska Range, Alaska: Geological Society of America Abstracts with Programs, v. 49, no. 6, https://doi.org/10.1130/abs/2017AM 2307791
- Weber, F.R., and Turner, D.L., 1977, A late Tertiary thrust fault in the central Alaska Range: U.S. Geological Survey Circular 751-B, p. B66-B67.
- Wesnousky, S.G., 1988, Seismological and structural evolution of strike-slip faults: Nature, v. 335, no. 6188, p. 340–343, https://doi.org/10.1038/335340a0.
- Whipple, K.X., and Dunne, T., 1992, The influence of debris-flow rheology on fan morphology, Owens Valley, California: Geological Society of America Bulletin, v. 104, no. 7, p. 887–900, https://doi.org/10.1130/0016-7606(1992)104<0887:TIODFR>2.3.CO;2.
- Wilson, F.H., Hults, C.P., Mull, C.G., and Karl, S.M., comps., 2015, Geologic map of Alaska: U.S. Geological Survey Scientific Investigations Map 3340, pamphlet 196 p., 2 sheets, scale 1:1,584,000, http://dx.doi.org/10.3133/sim3340.
- Wolf, R.A., Farley, K.A., and Silver, L.T., 1996, Helium diffusion and low temperature thermochronometry of apatite: Geochimica et Cosmochimica Acta, v. 60, p. 4231–4240, https://doi.org /10.1016/S0016-7037(96)00192-5.
- Yin, A., Rumelhart, P.E., Butler, R., Cowgill, E., Harrison, T.M., Foster, D.A., Ingersoll, R.V., Zhang, Q., Zhou, X.Q., Wang, X.F., Hanson, A., and Raza, A., 2002, Tectonic history of the Altyn Tagh fault system in northern Tibet inferred from Cenozoic sedimentation: Geological Society of America Bulletin, v. 114, p. 1257–1295, https://doi.org/10.1130/0016-7606(2002)114<1257: THOTAT>2.0.CO;2.
- Yin, A., Dang, Y.Q., Wang, L.C., Jiang, W.M., Zhou, S.P., Chen, X.H., Gehrels, G.E., and McRivette, M.W., 2008, Cenozoic tectonic evolution of Qaidam basin and its surrounding regions (Part 1): The southern Qilian Shan-Nan Shan thrust belt and northern Qaidam basin: Geological Society of America Bulletin, v. 120, p. 813–846, https://doi.org/10.1130 /B26180.1.